Overcoming Entropic Barriers by Capacity Hopping

Jackson Loper,[1, a)] Guangyao Zhou,[2, a)] and Stuart Geman[2]

[1)] *Data Science Institute, Columbia University, New York, NY, USA*

[2)] *Division of Applied Mathematics, Brown University, Providence, RI, USA*

(Dated: October 12, 2018)

We present Capacity Hopping (CHop), a method for estimating hitting probabilities of various targets in molecular dynamics simulations, for regions with golf-course potentials. CHop is based on a novel theoretical analysis of regions with golf-course potentials. Due to entropic effects, a system may spend significant time in such regions, just as enthalpic effects may cause a system to spend significant time trapped in local energetic minima. Many advances have been made in the theoretical analysis of local minima, but there has been little study of regions with golf-course potentials. Experimental evidence suggests that these regions are ubiquitous in biomolecular systems, and often characterize the rate-limiting step of biomolecular processes. In this paper, we investigate hitting probabilities of various targets inside these regions. We show that these regions are characterized by *approximately constant hitting probabilities* away from the target sets, and connect these hitting probabilities to *capacities* of local sets around the targets. Using these theoretical results and a new capacity estimation algorithm, we develop CHop, a method for estimating the approximately constant hitting probabilities. Numerical experiments on a toy model with a golf-course potential show that CHop is nearly as accurate as naive simulations in estimating hitting probabilities, but 750 times faster.

[a)] These two authors contributed equally

I. INTRODUCTION

Molecular dynamics simulations help us understand a diverse range of biomolecular processes, including the folding of macromolecules into their native configurations[34] and the conformational changes involved in their functioning[19]. Since their first introduction in the 1970s[26,42], substantial increase in speed and accuracy of molecular dynamics simulations has been achieved. However, we are still severely limited in the timescale we can access. Even with specialized hardwares, we can only achieve atomic-level simulations on timescales as long as milliseconds[13], while the timescales for various biomolecular processes vary widely, and can last for seconds or longer[28,48]. The challenges of molecular dynamics result from the complicated energy landscapes associated with different biomolecular systems, and can be summarized by two main difficulties: the difficulty of escaping local minima (the "enthalpic" effects), and the difficulty of reaching a small number of target configurations out of a vast number of possible configurations (the "entropic" effects).

Great efforts have been put into extending the timescale accessible by molecular dynamics simulations. A lot of methods focus on enhanced sampling, with simulated annealing[23], genetic algorithms[17] and parallel tempering[36] as representatives. However, dynamics is destroyed in these methods, and additional work[2,20,47,49] is needed in order to recover the kinetic information of the system, usually under the framework of kinetic transition networks[29,41] or Markov State Models[10,21,30]. When focusing directly on kinetics, the foundational work is transition state theory[9,16,45]. Various other methods build on top of this, including transition path sampling[7,12], transition interface sampling[38], and the more recent transition path theory[14,15]. The essential idea here is to provide information about the reaction rates between different states, which can then be used under the framework of kinetic transition networks[29,41] or Markov State Models[10,21,30] to understand the kinetics of the system. In addition, different accelerated molecular dynamics methods[32](hyperdynamics[39], parallel replica[40] and temperature-accelerated dynamics[35]) aim at directly accelerating the molecular dynamics simulations, by either smoothing the energy landscape, exploring energy basins in parallel, or raising the temperature while maintaining the correct dynamics. We refer the readers to some other reviews[11,24,32] for a more comprehensive picture of this area.

Careful inspection of the existing methods shows that a majority of the previous developments focus on the enthalpic effects, where the central picture consists of an energy

landscape with a multitude of local minima separated by high energetic barriers. A less studied picture involves the entropic effects, where we have large flat regions on the energy landscape with essentially no local minima. Here we focus on a particular kind of entropic effect: regions on the energy landscape with "golf-course" potentials.

A golf-course potential commonly takes place in high-dimensional configuration spaces. It features a large region and several small targets within the region. Away from the targets, the potential energy is relatively flat. Near the targets, the energy may be intricate, jagged, and feature steep local minima. Golf-course potentials are ubiquitous in biomolecular systems. For example, in folding-like dynamics (such as RNA folding or protein folding), it is thought that "folding rates are controlled by the rate of diffusion of pieces of the open coil in their search for favorable contacts" and "the vast majority of the space covered by the energy landscape must actually be flat."[27]. Experimental evidence shows that exploration of regions with golf-course potentials forms the rate-limiting step for a variety of processes.[18,22,33,37]

The difficulty for dealing with golf-course potentials has long been identified. In previous works[4,25,46], it's pointed out that enhanced sampling methods such as simulated annealing and parallel tempering work poorly for golf-course potentials. In accelerated molecular dynamics[35], the authors refer to this problem as the "low barrier problem". In the review[11], the author takes a largely pessimistic view on this subject: "If these processes are intrinsically slow, i.e. require an extensive sampling of state space" (which is indeed the case in the presence of golf-course potentials), "not much can be done to speed up their simulation without destroying the dynamics of the system."

In this paper, we argue for a new point of view: the long timescales involved in golf-course potentials can be a blessing rather than a curse. Indeed, if the targets are sufficiently small and the potential energy is sufficiently flat, the system must reach local equilibrium before it hits one of the targets. The exact initial condition within the region becomes irrelevant. As a consequence, the hitting probabilities are approximately constant for nearly all initial conditions in the region.

Under these conditions, we present theoretical results showing that these hitting probabilities can be approximated using only local information from the vicinities of the targets, coming in the form of "capacities". The capacities can be estimated by performing simulations around the target regions, without ever needing to simulate trajectories through the large flat region. This provides us with a computationally feasible way to estimate the ap-

proximately constant hitting probabilities away from the targets in regions with golf-course potentials. These hitting probabilities can help us understand various kinetic aspects of the system, e.g. important intermediates and folding pathways in the context of folding, by looking at the sequence of key configurations visited in the simulations.

The contributions of this paper are twofold:

Theory: We present new theoretical results about regions with golf-course potentials. We show that these regions are characterized by approximately constant hitting probabilities. We then demonstrate that these probabilities can be approximated using the capacities of local sets around the targets.

Application: Inspired by the theoretical results, we present CHop as a general method to estimate hitting probabilities in regions with golf-course potentials. We verify the effectiveness of CHop through extensive numerical experiments.

The rest of the paper is organized as follows. In Section II, we present a toy model with a golf-course potential. This example will run across the entire paper as a central thread for our theoretical and numerical analysis. In Section III, we present our theoretical results. We propose the concept of ε-flatness to capture the idea that hitting probabilities remain approximately a constant, and establish the ε-flatness of the toy model in Theorem 1. We make further connections of the approximately constant hitting probabilities to capacities of local sets around the targets in Corollary 1, for general stationary reversible SDEs. In Section IV, we talk about applications. We propose CHop as a general method for estimating hitting probabilities in regions with golf-course potentials, and discuss the central computational issue of CHop: the efficient estimation of the capacities. We present extensive numerical experiments and results in Section V to demonstrate the effectiveness of CHop, before giving conclusions and future directions in Section VI.

II. A TOY MODEL

To concretely demonstrate the CHop method, we introduce a simple toy model with a golf-course potential. This model features a high-dimensional configuration space containing two small target regions, A and B. Away from the targets, the potential energy is completely flat. To further simplify the analysis and facilitate numerical validation, we will assume all

sets of interest are spheres. The resulting model is perhaps the simplest possible example of a dynamics with golf-course qualities.

We will now give a formal definition of the model. The dynamics will take place inside the unit ball, $\Omega = \mathcal{B}(0,1)$, where $\mathcal{B}(x,r) \triangleq \{y : ||y-x|| < r\}$. The configuration space will also feature two important target regions:

$$A \triangleq \mathcal{B}(x_A, r_A)$$
$$B \triangleq \mathcal{B}(x_B, r_B)$$

where $x_A, x_B \in \Omega$. Given an initial condition $X_0 \in \Omega \backslash (A \cup B)$, we will be be interested to know whether the dynamics carry the system into A or B first. These dynamics will be defined in terms of a d-dimensional Brownian motion W_t, according to

$$\mathrm{d}X_t = -\nabla U(X_t)\mathrm{d}t + \mathrm{d}W_t \tag{1}$$

with reflecting boundary at the boundary of Ω. We will require that the potential energy U is differentiable and flat outside of a region around the targets. In particular, we will fix $d_A > r_A$ and $d_B > d_B$ and require that $U(x) = 0, \forall x \notin \mathcal{B}(x_A, d_A) \cup \mathcal{B}(x_B, x_B)$. To simplify the theorems, we also require that the surface of Ω is part of the flat region, i.e. $||x_A|| + d_A, ||x_B| + d_B < 1$. We also assume that the two target regions do not overlap: $\bar{\mathcal{B}}(x_A, d_A), \bar{\mathcal{B}}(x_B, x_B)$ are disjoint, where $\bar{\mathcal{B}}()$ denotes the closure of $\mathcal{B}()$.

This toy model encapsulates the essential characteristics of entropic effects: if r_A, r_B are small, the trajectory of X will generally be spent well away from A or B, in the large flat region of the energy landscape that separates A from B. The nontrivial energy landscapes in the immediate vicinity of A and B reflect the local nature of energetic interactions in the system under biological conditions, and the reflecting boundary $\partial\Omega$ captures the notion that not all configurations for the biomolecular system are sensible, because of, for example, the limits on bond lengths, angles and dihedral angles in the case of RNA molecules.

III. THEORY: ε-FLATNESS AND CHOP PROBABILITIES

With this toy model in mind, we now turn to the general results of this paper. In general, we will assume the underlying physical process governing the macromolecule is a stationary reversible diffusion process in the configuration space Ω, with invariant measure

$\mu = e^{-U(x)}\mathrm{d}x$. In particular, the dynamics will be defined in terms of a d-dimensional Brownian motion W_t, according to

$$\mathrm{d}X_t = b(X_t)\mathrm{d}t + \sigma(X_t)\mathrm{d}W_t \tag{2}$$

where $b : \Omega \to \mathbb{R}^d$ and $\sigma : \Omega \to \mathbb{R}^{d\times m}$ are differentiable vector-valued and matrix-valued functions. We refer the reader to Appendix A for a detailed account of stationary reversible diffusion processes.

As in the toy model, we will be interested in two target regions, $A, B \subset \Omega$. Given an initial condition $X_0 \in \Omega\backslash(A \cup B)$, we will be be interested to know whether the dynamics carry the system into A or B first. That is, we are interested in the hitting probabilities

$$h_{A,B}(x) \triangleq \mathbb{P}(X_{\tau_{A\cup B}} \in A | X_0 = x)$$

where τ_S indicates the time when the process first hits a set S, i.e. $\tau_S \triangleq \inf\{t \geqslant 0 : X_t \in S\}$. Thus $h_{A,B}(x)$ indicates the probability that $\{X_t\}_{t\geq 0}$ hits A before B given that it starts at $x \in \Omega$.

Our theoretical inquiry began with an intuition. Let us consider the case that A and B are very small relative to Ω. Let us also assume that U is sufficiently flat in $\Omega/(A \cup B)$. In this case, for any starting point $x \in \Omega/(A \cup B)$, we would reach local equilibrium before we hit the targets. In that case the hitting probability $h_{A,B}(x)$ should not depend upon the initial condition. That is, $h_{A,B}(x)$ should be approximately *constant* for all initial conditions x which are reasonably far away from A and B. In addition, since we reach local equilibrium before we hit the targets, the exact internal structure of $\Omega/(A \cup B)$ away from A and B may not be important. We might therefore hope that the hitting probabilities could be accurately estimated without looking at this internal structure. In summary, it seems that

1. There should be some constant $\bar{h}$ such that $\bar{h}_{A,B} \approx h_{A,B}(x)$ for all initial conditions x which are reasonably far away from A and B.

2. It should be possible to estimate $\bar{h}$ using only knowledge of the dynamics in the local regions around A, B.

In what follows, we make the above intuitions rigorous. First, for our toy model we establish that the hitting probabilities are indeed constant away from A, B. We see the kinds of arguments that would be necessary to establish this result for other models. Second, we

turn to the general case. Whenever hitting probabilities are approximately constant in a region away from A, B, we show that the value of this constant can be determined by looking only at the dynamics of local regions around A, B. In particular, we show that the key quantity is what is known as the "capacity" of local sets around the targets.

A. Approximately Constant Hitting Probability

In this section, we introduce the concept of ε-flatness, establish it for our toy model, and see when it will hold in general models. We introduce this concept to formally define what it would mean that the hitting probability function $h_{A,B}(x)$ is "approximately constant" in a given region.

Definition 1. *(ε-flatness) For any function h on Ω and an $\varepsilon > 0$, a set $M \subset \Omega$ is ε-flat for the function h iff $\sup_{x,y\in M} |h(x) - h(y)| < \varepsilon$.*

Note that if M is ε-flat for h, then we can always find some constant $\bar{h}$ so that $\sup_{x\in M} |\bar{h} - h(x)| < \varepsilon$ for all $x \in M$. Simply pick $\bar{h}$ to be $h(x)$ for any $x \in M$.

For the toy model, we can see how ε-flatness applies to hitting probabilities. Let us recall the notation of the toy model. We have two sets, $A = \mathcal{B}(x_A, r_A), B = \mathcal{B}(x_B, r_B)$ in d-dimensional space. The dynamics are governed by a potential energy which is flat outside of $\mathcal{B}(x_A, d_A) \cup \mathcal{B}(x_B, d_B)$, where $d_A > r_A, d_B > r_B$. We now introduce a third layer of neighborhoods around the target regions. We fix some $r_{\tilde{A}} > d_A, r_{\tilde{B}} > d_B$ and define $\tilde{A} = \mathcal{B}(x_A, r_{\tilde{A}}), \tilde{B} = \mathcal{B}(x_B, r_{\tilde{B}})$. We will show conditions such that the hitting probabilities are constant away from $\tilde{A}, \tilde{B}$. In particular, the probabilities must be constant as long as when the targets A, B are sufficiently small or the dimension is high:

Theorem 1. *For any fixed value of $d \geq 3$ and $r_{\tilde{A}}, r_{\tilde{B}}, \varepsilon > 0$, there exists a constant $c = c(d, r_{\tilde{A}}, r_{\tilde{B}}, \varepsilon)$ such that if $d_A, d_B < c$ then $\mathcal{B}(0,1)/(\tilde{A} \cup \tilde{B})$ is ε-flat for the function $h_{A,B}(x)$. Likewise for any fixed value of $d_A, r_{\tilde{A}}, d_B, r_{\tilde{B}}, \varepsilon > 0$, there exists a constant $c = c(d_A, r_{\tilde{A}}, d_B, r_{\tilde{B}}, \varepsilon)$ such that if $d \geq c$ then $\mathcal{B}(0,1)/(\tilde{A} \cup \tilde{B})$ is ε-flat for the function $h_{A,B}(x)$.*

We defer the proof of this theorem to Appendix C. Inspection of the proof demonstrates that the key for establishing ε-flatness is a proper separation of time scales: it takes a short time for the process $\{X_t\}_{t\geq 0}$ to reach local equilibrium in $\mathcal{B}(0,1)/(\tilde{A} \cup \tilde{B})$ and a long time

for the process $\{X_t\}_{t\geq 0}$ to hit the targets A and B. Any model with these characteristics will feature ε-flat hitting probabilities.

B. Estimating Constant Hitting Probability Using Local Information

In this section, we show that hitting probabilities can be determined using only local information around the targets, as long as the hitting probability function enjoys ε-flatness. In particular, it will be sufficient to calculate the "capacities" for local sets around the targets. This is defined as follows. Let $\{X_t\}_{t\geq 0}$ be a reversible stationary process governed by Equation (2). Then for $A \subset \tilde{A} \subset \Omega$, the capacity $\text{cap}(A, \tilde{A})$ for X is defined as

$$\text{cap}(A, \tilde{A}) \triangleq \frac{1}{2}\int_{\Omega} ||\sigma(x)\nabla h_{A,\tilde{A}^c}(x)||^2 e^{-U(x)}\mathrm{d}x$$

Recall that $h_{A,\tilde{A}^c}(x)$ denotes the probability that the dynamics will hit A before hitting $\tilde{A}^c$, given that $X_0 = x \in \tilde{A}\backslash A$. We refer the reader to Appendix A for more details on capacity and the the related concept of Dirichlet form.

In the presence of ε-flatness, these capacities are intimately related to hitting probabilities:

Theorem 2. *Let $\{X_t\}_{t\geq 0}$ be a reversible stationary diffusion on Ω governed by Equation (2). Let $A \subset \tilde{A} \subset \Omega, B \subset \tilde{B} \subset \Omega$. If $\tilde{A}, \tilde{B}$ are disjoint and $\Omega\backslash(\tilde{A}\cup\tilde{B})$ is ε-flat for the hitting probabilities $h_{A,B}(x)$, then*

$$\sup_{x\in M}\left| h_{A,B}(x) - \frac{\text{cap}(A,\tilde{A})}{\text{cap}(A,\tilde{A}) + \text{cap}(B,\tilde{B})}\right| \leqslant \varepsilon + \sqrt{\frac{\varepsilon}{2}}$$

for any $\varepsilon \in [0, 2/9]$.

We defer the proof to Appendix B. This theorem generalizes naturally to the case of multiple targets. For a collection of targets with neighborhoods, we first define the approximate probability estimates, which we call "CHop probabilities."

Definition 2. *Let $\{X_t\}_{t\geq 0}$ be a stationary reversible diffusion process on Ω. Pick $A_1 \cdots A_n \subset \Omega$ and $\tilde{A}_1 \cdots \tilde{A}_n \subset \Omega$ such that $A_k \subset \tilde{A}_k$. Then the **CHop Probability** for the set A_k (given all the other sets $A_1 \cdots, A_{k-1}, A_{k+1}, \cdots A_n \subset \Omega$ and $\tilde{A}_1 \cdots \tilde{A}_n \subset \Omega$) is given by*

$$p_{A_k} = \frac{\text{cap}(A_k, \tilde{A}_k)}{\sum_{i=1}^n \text{cap}(A_i, \tilde{A}_i)}, k = 1, \ldots, n$$

In terms of these definitions, Theorem 2 then yields:

Corollary 1. *Let $u_k = h_{A_k, \cup_{i \neq k} A_i}$ denote the probability the process hits A_k before the other target sets. Fix any $\varepsilon \in \left(0, \frac{2}{9}\right]$. If $M = \Omega \backslash \bigcup_{k=1}^{n} \tilde{A}_k$ is ε-flat for the functions $\{u_k\}_{k \in 1,\ldots,n}$ then each u_k is well-approximated by the corresponding CHop Probability:*

$$\sup_{x \in M} |u_k(x) - p_{A_k}| \leqslant \varepsilon + \sqrt{\frac{\varepsilon}{2}}, k = 1, \ldots, n$$

This corollary follows immediately from Theorem 2 and additivity of the capacity (Proposition **??** in Appendix A).

IV. APPLICATION: CHOP METHOD AND CAPACITY ESTIMATION

Inspired by the theoretical analysis above, we introduce the CHop method as a way to study kinetic aspects of biomolecular systems by efficiently dealing with regions with golf-course potential. We present the high-level idea of the CHop method, and give a detailed account of the key computational issue of the CHop method, the efficient estimation of capacities. A general framework based on a simple lemma is given for capacity estimation, and the associated challenges are discussed. To demonstrate this framework, we give an outline of a flexible and general-purpose algorithm for capacity estimation, and make some concrete choices to show how exactly the algorithm works in the case of our toy model. This will serve as the basis for the numerical experiments and results in Section V.

Recall that in the previous section on theory, we made the following two key points:

1. We can establish ε-flatness in regions with a golf-course potential, and the hitting probabilities of the various targets remains approximately a constant over a large part of the flat region.

2. The approximately constant hitting probabilities can be accurately estimated using CHop probabilities, which depend on capacities that can be determined solely based on the local information around the targets.

The above theoretical insights provide us with an efficient way to deal with golf-course potentials, so that we can get information of the biomolecular system on a much longer time-scale: we make use of our knowledge of the targets (which is typically available, e.g. in the

form of different secondary structures for RNAs) to carry out local simulations around the targets for the estimation of capacites. Capacities can then be used to calculate the CHop probabilities, which give us an accurate estimate of the approximately constant hitting probabilities. This enables us to study kinetics of the biomolecular systems by looking at sequences of key configurations visited in molecular dynamics simulations, which is the essence of the CHop method.

A. CHop Method

Let $\{X_t\}_{t\geq 0}$ by a process governed by Equation 2 on Ω. Let $A_1 \cdots A_n \subset \Omega$ denote the target sets of interest. On a high-level, the CHop method is a method for approximating hitting probabilities for systems initialized inside large, flat regions. It consists of the following steps:

1. Identify suitable sets $\tilde{A}_k \subset \Omega$ where $A_k \subset \tilde{A}_k, k = 1, \cdots, n$, such that we can establish the ε-flatness of $M = \Omega \backslash \bigcup_{k=1}^{n} \tilde{A}_k$ for hitting probability functions $h_{A_k, \cup_{i\neq k} A_i}(x)$.

2. Estimate the capacities $\mathrm{cap}(A_k, \tilde{A}_k)$, from which we can derive the CHop probabilities

$$p_{A_k} = \frac{\mathrm{cap}(A_k, \tilde{A}_k)}{\sum_{i=1}^{n} \mathrm{cap}(A_i, \tilde{A}_i)}, k = 1, \ldots, n$$

3. For any initial condition $x \in M$, approximate the hitting probability $h_{A_k, \cup_{i\neq k} A_i}(x)$ with the CHop probability p_{A_k}.

To make the CHop method practical, we need to be able to estimate the capacities accurately and efficiently. This would be our topic for the rest of this section.

B. Estimation of Capacities

We start our discussion on estimating the capacities with a simple lemma:

Lemma 1. *For a stationary reversible diffusion process X_t in Ω with invariant measure $\mu = e^{-U(x)}\mathrm{d}x$ and diffusion matrix $a(x)$, given non-empty sets $A \subset G \subset \tilde{G} \subset \tilde{A}$ with smooth*

boundaries, the capacity $\mathrm{cap}(A, \tilde{A})$ *can be calculated by*

$$\begin{aligned}\mathrm{cap}(A, \tilde{A}) = &\int_{\partial \tilde{G}} h_{A,\tilde{A}^c}(x) e^{-U(x)} [a(x) \nabla h_{G,\tilde{G}^c}(x)]^T \boldsymbol{n}(x) \mathrm{d}S \\ &- \int_{\partial G} h_{A,\tilde{A}^c}(x) e^{-U(x)} [a(x) \nabla h_{G,\tilde{G}^c}(x)]^T \boldsymbol{n}(x) \mathrm{d}S\end{aligned}$$

where $\boldsymbol{n}(x)$ *in the integral is taken as the outward-facing normal vector at point* x *on the surface we are integrating on, and* $\mathrm{d}S$ *represents the surface integral.*

We defer the proof of this lemma to Appendix D. This lemma provides us with a general framework for estimating the capacities. In particular, we can approximate the integrals in the lemma with a Monte Carlo method, as long as we can overcome three challenges:

1. To sample $y_1, y_2, \cdots y_m$ on ∂G and $\tilde{y}_1, \tilde{y}_2 \cdots \tilde{y}_n$ on $\partial \tilde{G}$ according to the invariant measure $e^{-U(x)} \mathrm{d}x$ restricted on $\partial G, \partial \tilde{G}$ and compute the surface areas $|\partial G|$ and $|\partial \tilde{G}|$
2. To estimate $\nabla h_{G,\tilde{G}^c}$ on ∂G and $\partial \tilde{G}$
3. To estimate $h_{A,\tilde{A}^c}$ on ∂G and $\partial \tilde{G}$

With these pieces in place, using the lemma, we can approximate the capacity by

$$\begin{aligned}\mathrm{cap}(A, \tilde{A}) \approx \quad &|\partial \tilde{G}| \frac{\sum_i^n h_{A,\tilde{A}^c}(\tilde{y}_i)[a(\tilde{y}_i) \nabla h_{G,\tilde{G}^c}(\tilde{y}_i)]^T \mathbf{n}(\tilde{y}_i)}{\sum_i^n e^{U(\tilde{y}_i)}} \\ &- |\partial G| \frac{\sum_i^m h_{A,\tilde{A}^c}(y_i)[a(y_i) \nabla h_{G,\tilde{G}^c}(y_i)]^T \mathbf{n}(y_i)}{\sum_i^n e^{U(y_i)}}\end{aligned} \tag{3}$$

The first challenge (sampling of points) can be addressed using existing methods, e.g. an importance sampling based approach, and is further simplified by the fact that we have the freedom to pick G and $\tilde{G}$. In some special cases (e.g. the toy model), it's not hard to pick $G, \tilde{G}$ in such a way that we can get exact samples from the invariant measure $e^{-U(x)} \mathrm{d}x$.

The second challenge (estimation of $h_{G,\tilde{G}}$) can be addressed by making judicious choice of G and $\tilde{G}$ so that $\nabla h_{G,\tilde{G}^c}$ is relatively straightforward to compute. For example, in the general case, we can pick $\tilde{G}$ to be a small dilation of G (i.e. $\tilde{G} = \{x : \exists y \in G : |x - y| < \varepsilon\}$), so that the gradient can be well approximated by the surface normal of ∂G and $\partial \tilde{G}$. In some special cases (e.g. the toy model), we can even get analytical formulas for $\nabla h_{G,\tilde{G}^c}$.

The third challenge (estimation of $h_{A,\tilde{A}^c}$) requires more of a customized solution. The probabilistic interpretation of $h_{A,\tilde{A}^c}$ allows us to estimate it with local simulations. Since $\tilde{A}$ is a small, local space, $\tau_{A \cup \tilde{A}}$ will be relatively small, and we can successfully complete these simulations. In theory it would be possible to use many such simulations to estimate $h_{A,\tilde{A}^c}$. However, there are two main issues which tend to make this approach infeasible:

1. *Extreme probabilities.* If $h_{A,\tilde{A}^c}(x)$ is close to 0 or 1, it becomes much harder to obtain accurate estimates, since we would have to run a large number of trial simulations in order to get a good estimate of the hitting probability.

2. *Many starting points required.* The Monte Carlo approach requires us to run simulations for a collection of starting points on a particular surface, which in turn requires us to run a huge number of trial simulations.

In this paper, we propose a flexible and general-purpose method for the efficient estimation of $h_{A,\tilde{A}^c}(x)$ on a surface ∂S, where $A \subset S \subset \tilde{A}$. The basic idea is to approximate the continuous diffusion with a discrete Markov process, and make use of the corresponding embedded Markov chain to estimate the hitting probability. In this approach, we only need to estimate the transition probabilities between different discretized states. The local transition probabilities of the Markov process tend to be much less extreme, solving issues of extreme probabilities. This approach also allows us to simultaneously estimate the hitting probabilities of all the discretized states on ∂S, which makes it computationally tractable to deal with all of the starting points that we need.

The method is closely related to milestoning[3,5,44] and Markov state models[10,21,30], yet is more specialized and tailored to the problem at hand. In particular, we seek not to approximate the underlying process, but only to understand the hitting probability. Our goal is to make the method adaptive to the energy landscape, without the need for any prior knowledge. To this end, we evolve an ensemble of samples, and use a clustering-based approach to define the states.

The method has three main stages: determining the discretized states, running local simulations to estimate the transition probabilities, and estimating the hitting probabilities. The method is detailed in Appendix E.

C. Outline of the Capacity Estimation Algorithm

In what follows, we put all the pieces from our previous discussions together, and present the outline of a flexible and general purpose capacity estimation algorithm:

Algorithm 1. *Estimating* $\mathrm{cap}(A, \tilde{A})$ *for* $A \subset \tilde{A} \subset \Omega$

Input: *$A \subset \tilde{A} \subset \Omega$ and a stationary reversible diffusion process $\{X_t\}_{t\geq 0}$ in Ω with invariant measure $\mu = e^{-U(x)}\mathrm{d}x$ and diffusion matrix $a(x)$*

Output: *An estimated value of* $\mathrm{cap}(A, \tilde{A})$

1. *Pick $G, \tilde{G}$ with smooth boundaries, s.t. $A \subset G \subset \tilde{G} \subset \tilde{A}$*

2. *Estimate the surface areas $|\partial G|$ and $|\partial \tilde{G}|$*

3. *Sample $y_1, y_2, \cdots y_m$ on ∂G and $\tilde{y}_1, \tilde{y}_2 \cdots \tilde{y}_n$ on $\partial \tilde{G}$ according to the invariant measure $e^{-U(x)}\mathrm{d}x$ restricted on $\partial G, \partial \tilde{G}$, and estimate $h_{A,\tilde{A}^c}(y_i), i = 1, \cdots, m$ and $h_{A,\tilde{A}^c}(\tilde{y}_i), i = 1, \cdots, n$ using Algorithm 2 in Appendix E applied to the cases $S = G$ and $S = \tilde{G}$*

4. *Estimate $\nabla h_{G,\tilde{G}^c}(y_i), \boldsymbol{n}(y_i), i = 1, \cdots, m$ and $\nabla h_{G,\tilde{G}^c}(\tilde{y}_i), \boldsymbol{n}(\tilde{y}_i), i = 1, \cdots, n$, where $\boldsymbol{n}(x)$ denotes the the outward-facing normal vector at point x on the corresponding surfaces*

5. *Estimate* $\mathrm{cap}(A, \tilde{A})$ *using the formula given in Equation 3*

To understand this algorithm more concretely, let us now use it to estimate $\mathrm{cap}(A, \tilde{A})$ in the setup of the toy model. Here we can use the simple geometry and the exactly flat energy landscape of the toy model to our advantage. We follow the outline given in Algorithm 1.

1. We pick $G = \dot{A}$ and $\tilde{G} = \tilde{A}$, where $\dot{A}$ and $\tilde{A}$ are as in our toy model.

2. The surfaces areas can be easily calculated analytically as

$$|\partial G| = \frac{2\pi^{\frac{d}{2}}}{\Gamma(\frac{d}{2})} d_A^{d-1}, |\partial \tilde{G}| = \frac{2\pi^{\frac{d}{2}}}{\Gamma(\frac{d}{2})} \tilde{r}_A^{d-1}$$

3. The restrictions of the invariant measure $e^{-U(x)}\mathrm{d}x$ on ∂G and $\partial \tilde{G}$ are simply uniform distributions on these two spheres, and we can generate exact samples on these two spheres. Since $\tilde{G} = \tilde{A}$ it is straightforward to use the probabilistic interpretation of h to see that $h_{A,\tilde{A}^c}(x) = 0, \forall x \in \partial \tilde{G}$, so we only need to apply Algorithm 2 to the case of $S = G = \dot{A}$. Following the notations used in Algorithm 2, assume we get N_p samples $z_1, \cdots, z_{N_p}$, and the hitting probability vector $u^{(m)}$ for the N_b clusters on $\partial S_m = \partial G$, we have the estimates given in Equation E1

4. $h_{G,\tilde{G}^c}$ can be identified analytically as the harmonic function on $\tilde{G}/G$[43]

$$h_{G,\tilde{G}^c}(x) = \frac{1}{d_A^{2-d} - r_{\tilde{A}}^{2-d}} \|x - x_A\|^{2-d} - \frac{r_{\tilde{A}}^{2-d}}{d_A^{2-d} - r_{\tilde{A}}^{2-d}}$$

As a result, the gradient is given by

$$\nabla h_{G,\tilde{G}^c}(x) = \frac{2-d}{d_A^{2-d} - r_{\tilde{A}}^{2-d}} \|x - x_A\|^{1-d} \frac{x - x_A}{\|x - x_A\|}$$

Note that on both $\partial\tilde{G}$ and ∂G, the outward normal is given by $\mathbf{n}(x) = \frac{x-x_A}{\|x-x_A\|}$, so

$$\mathbf{n}(x)^T \nabla h_{G,\tilde{G}^c}(x) = \frac{2-d}{d_A^{2-d} - r_{\tilde{A}}^{2-d}} \|x - x_A\|^{1-d} = \begin{cases} \frac{(2-d) r_{\tilde{A}}^{1-d}}{d_A^{2-d} - r_{\tilde{A}}^{2-d}} & \text{if } x \in \partial\tilde{G} \\ \frac{(2-d) d_A^{1-d}}{d_A^{2-d} - r_{\tilde{A}}^{2-d}} & \text{if } x \in \partial G \end{cases}$$

5. Finally, note that $U(x) = 0$ and $a(x) = I$ for $x \in \partial\tilde{G}, \partial G$. Plugging these into Equation (3), we obtain the approximation

$$\text{cap}(A, \tilde{A}) \approx \frac{2\pi^{\frac{d}{2}}}{\Gamma(\frac{d}{2})} \frac{d-2}{d_A^{2-d} - r_{\tilde{A}}^{2-d}} \frac{1}{N_p} \sum_{k=1}^{N_b} n_k u_k^{(m)} \tag{4}$$

where $n_k, k = 1, \cdots, N_b$ is the number of samples in $z_1, \cdots, z_{N_p}$ that belong to cluster k on $\partial S = \partial G = \partial\dot{A}$

V. NUMERICAL EXPERIMENTS AND RESULTS

In this section we use simulations to test the limits of our theories and algorithms. In this work we have made three claims, each of which can be we can test empirically:

- In regions with golf-course potentials the hitting probabilities are approximately constant away from the targets.
- In regions with golf-course potentials, the value of this constant can be well-approximated using CHop probabilities, which are defined in terms of local capacities.
- The CHop capacity estimation algorithm is efficient and accurate

In what follows, we present experimental results with our toy model, using both a flat and a nontrivial energy landscape, to verify each of these aspects. All the results presented in this section can be easily reproduced. For detailed instructions, please refer to `https://github.com/StannisZhou/capacity_hopping`.

A. Sanity Checks on Flat Energy Landscape

The first set of experiments are "sanity checks" designed to show that the CHop methods works in the simplest possible case. For these sanity checks, we work with a flat energy landscape in $\mathbb{R}^5$, where quantities of interest can be obtained in closed form. In particular, we look at the toy model with parameters !!!!

1. The hitting probabilities are approximately constant

The first sanity check tests the CHop idea at its most basic level: that the large flat region of a golf-course potential features constant hitting probabilities, i.e. ε-flatness. Theorem 1 shows that this must hold in the limiting regime of small r_A, r_B, but it is not obvious whether the parameters we use lie in that regime.

In the toy model, we see that the ε-flatness condition indeed holds, with $\varepsilon \approx .05$. We ran 2000 diffusion simulations at each of 100 randomly selected initial conditions in the "flat region" $\mathcal{B}(0,1) \setminus (\tilde{A} \cup \tilde{B})$. A histogram of these probabilities may be found in Figure 1. From this we see that the hitting probabilities in this region do not substantially depend upon the initial condition, all falling in the range $[0.2055, 0.2480]$.

2. The value of this constant is well-approximated using CHop probabilities

Our second check tests whether the CHop probabilities accurately approximate the hitting probabilities. For this problem, the relevant CHop probabilities can be computed in closed form:

$$p_A = \frac{\frac{1}{r_A^{2-d} - r_{\tilde{A}}^{2-d}}}{\frac{1}{r_A^{2-d} - r_{\tilde{A}}^{2-d}} + \frac{1}{r_B^{2-d} - r_{\tilde{B}}^{2-d}}} \tag{5}$$

According to this formula, the CHop probability is .2286. This is in good agreement with the average hitting probability .2236 found by direct simulation in the previous section.

3. CHop capacity estimation

Finally, we check the accuracy of the capacity estimation algorithm employed by CHop. We can get an analytical formula for the capacities in this case. We compare these exact

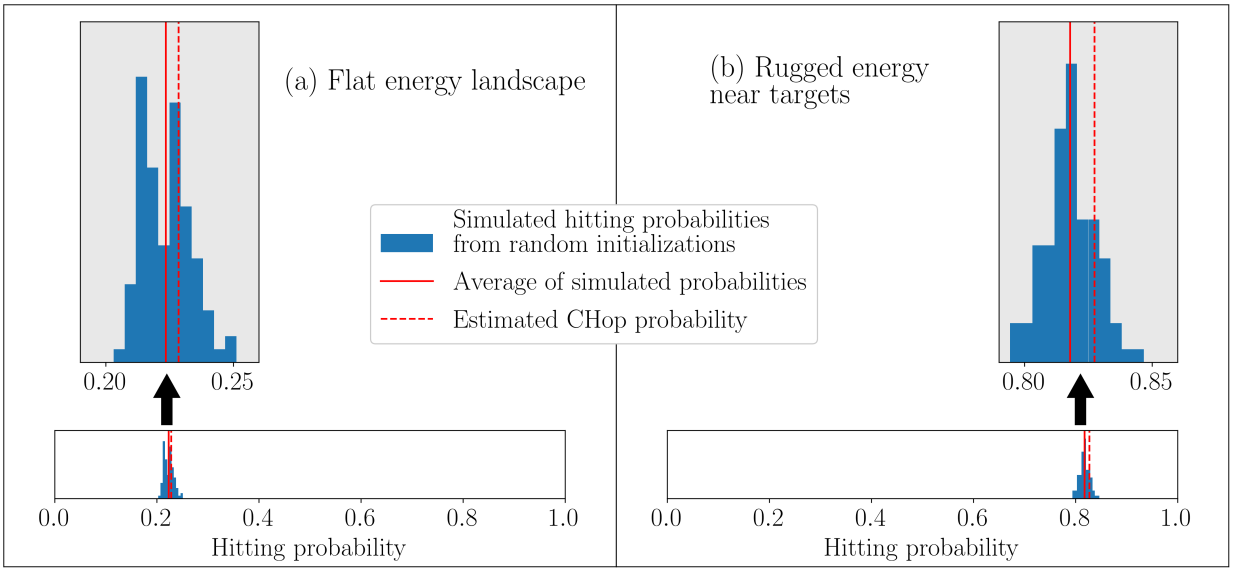

Figure 1. **Simulated hitting probabilities vs. CHop probabilities**. The CHop method accurately answers the question "where will we go next?" for a dynamics simulation initialized in a large, flat region of configuration space. We start by designating two target regions, A and B. For any given initial condition, our task is to determine the probability that we hit A first. We look at this question in the context of two different dynamics. In subfigure (a), we use the simplest possible dynamics: Brownian motion. In subfigure (b), we consider the case that the energy landscape U becomes complex and rugged near the targets of interest. In both cases we consider 100 random initial locations which are away from either target regions. For each initial condition, we conduct 2000 simulations to estimate the probability of hitting target A first. For both dynamics we see that the hitting probability is nearly constant for initial conditions which are away from the target regions. Furthermore, the value of this constant is well-approximated by the CHop estimates. These simulations show that the CHop probabilities are able to reconstruct a global property of the system, even though they completely invariant to the dynamics for the majority of configuration space. Indeed, the CHop probabilities can be computed using only small local simulations around each target, and do not require any simulations of trajectories that cross the large, flat region between A and B.

values with those estimated using the method outlined in Section IV C, with parameters $m = 2, n = 4, N_p = 100, N_b = 3, N_s = 1000$ and a time-step of 10^{-6}. We obtain the following results:

- $\text{cap}\left(A; \tilde{A}\right) =$!!!!, and our method obtained the estimate !!!!
- $\text{cap}\left(B; \tilde{B}\right) =$!!!!, and our method obtained the estimate !!!!

These show good agreement between the truth and our estimates.

B. Results on Nontrivial Energy Landscape

In this section, we apply the CHop method to a model with a nontrivial energy landscape around the targets. We see that our algorithm can accurately estimate the hitting probabilities while maintaining great advantage over the direct simulations in terms of speed.

We experimented with the toy model parameters with $d = 5$ and

$$x_A = \left(0.5 \;\; 0.6 \;\; 0.0 \;\; 0.0 \;\; 0.0\right), r_A = 0.02, d_A = 0.05, r_{\tilde{A}} = 0.1$$

for target A, and

$$x_B = \left(-0.7 \;\; 0.0 \;\; 0.0 \;\; 0.0 \;\; 0.0\right), r_B = 0.04, d_B = 0.075, r_{\tilde{B}} = 0.15$$

for target B. We refer the reader to Appendix F for more details.

1. The hitting probabilities are approximately constant

We again start by testing the basic idea of CHop: we use direct simulations to test the hypothesis that the hitting probabilities are relatively flat in away from the targets. The results can be seen in Figure 1. For every initial condition we tested, we found that the hitting probability fell in the interval $[0.7980, 0.8450]$, suggesting that the ε-flatness condition holds with $\varepsilon \approx .05$.

2. The value of this constant is well-approximated using CHop probabilities

Using the CHop capacity estimation procedure from Section IV C, we obtained an estimate of 0.8274 for the CHop probability of this model. This is in good agreement with

the average hitting probability .8180 found in our direct simulations. For the capacity estimation procedure, we used the parameters $m = 2, N_p = 5000, N_b = 10, N_s = 2000$ and a time-step of 10^{-7}. For the A capacity we used $n = 4$ and for the slightly larger B region we used $n = 5$.

3. CHop capacity estimation

In this case it is difficult to assess the accuracy of the CHop capacity algorithm. It is not possible to obtain exact values for the capacity. Therefore, we cannot directly test whether our algorithm is accurately estimating the capcities. However, as the last section showed, the CHop probabilities computed from our estimated capacities do seem to accurately reflect the true hitting probabilities. This offers some limited evidence that the estimated capacities are also accurate.

We can also test the speed of CHop capacity estimation algorithm. We compared the time it takes to estimate the hitting probabilities using direct simulations with the time our capacity estimation algorithm needs to estimate the capacities for all targets. Note that in order to make the direct simulations feasible for the 5-dimensional toy model we are working on, we made our best effort to make the direct simulation fast. We use an efficient walk-on-spheres method to simulate trajectories in the flat region,[6] JIT compilation to remove loop overhead, 24-CPU parallization, and a relatively coarse time step. The CPU times for the direct simulations and the CHop method are shown below:

Direct simulation: 89177.87 seconds (3715.74 seconds on a cluster of 24 CPUs). This quantity is the sum over the amount of time it took to run 2000 simulations for each of the 100 different initial locations, using a relatively coarse time step of 10^{-5}. These direct simulations are trivial to perform in parallel, assuring us that there was no significant overhead due to the parallelization.

CHop speed: 1055.55 seconds on a single CPU. In doing this we employed a time step which was 100 times more accurate than the one used for direct simulation (i.e. a timestep of 10^{-7}). Despite this, the CHop algorithm was three times faster on a single node than the direct method run on a cluster of 24 nodes.

This reflects an 85-fold acceleration. Furthermore note that the time-consuming elements

of the capacity estimation algorithm are "embarassingly parallelizable" and should be easy to further accelerate using parallelization. There was no need to do so in this case because we could easily run the CHop code on our laptops. However, larger scale problems would certainly benefit from this kind of acceleration.

The times reported above reflect a particular choice of parameters, but we found that the accuracy of the algorithm was fairly robust to choices of N_p, N_b and N_s. For example, we performed another experiment with time step of 10^{-6}, parameters of $m = 2, n = 4, N_p = 3000, N_b = 5, N_s = 1000$ for estimating the A capacity, and parameters of $m = 2, n = 5, N_p = 3000, N_b = 5, N_s = 1000$ for estimating the B capacity. The result was an estimate of 0.8420. This still agrees well with the direct simulations (indeed, there were some initial conditions for which the direct simulation hitting probability estimates agreed with this quantity almost exactly). Using these parameters, total computation time was reduced to 119.35 seconds, reflecting a 750-fold acceleration.

VI. CONCLUSIONS AND FUTURE DIRECTIONS

Using a golf-course energy landscape with multiple targets as a prototypical example, this paper gives new theoretical insights into the commonly encountered entropic barriers in molecular dynamics simulations, from the perspective of hitting probabilities of the targets. A new concept called ε-flatness is proposed to capture the idea of the hitting probabilities being approximately a constant in a set, and ε-flatness is established for a characteristic entropic barrier, our toy model. Further connections are made between the global hitting probabilities of the entropic barriers and the capacities of local sets around the targets, to facilitate the easy understanding of entropic barriers. Inspired by these theoretical developments, we propose CHop as a general and practical method for overcoming entropic barriers, together with an efficient algorithm to deal with the central computational issue of CHop, namely the estimation of capacities.

Extensive numerical results demonstrate that CHop is highly effective in the presence of entropic barriers, both in terms of accuracy and speed, yet future work remains. We see three directions as the most important in further developing the ideas set forth in this paper:

1. Move beyond the toy problem in this paper, and make CHop generally applicable to more realistic biomolecular systems. This involves identifying entropic barriers and

establishing their ε-flatness in a more general setting, and thinking carefully about the geometry of more realistic biomolecular systems to estimate the capacities of the sets around the targets. Some preliminary discussions are given in this paper, but more work is needed in order to get a clear understanding.

2. Get results concerning hitting times, in addition to the hitting probabilities talked about in the paper, so that we can fully recover the kinetic information of the system.

3. Think more about ways to model the configuration space as a hierarchical, nested golf-course, with each target as a mini golf-course inside a larger one, and apply CHop recursively so as to develop a complete model for biomolecular systems, much like kinetic transition networks[29,41] and Markov State Models[10,21,30]

Appendix A: Stationary Reversible Diffusion Processes

In this section, we set notation and review some properties of stochastic differential equations. Let $\{X_t\}_{t\geqslant 0}$ denote a stationary reversible diffusion process trapped in $\Omega \subset \mathbb{R}^d$ by reflecting boundaries, with continuous invariant density e^{-U}, satisfying

$$\mathrm{d}X_t = b(X_t)\mathrm{d}t + \sigma(X_t)\mathrm{d}W_t$$

where W is a d-dimensional Brownian motion and $b(\cdot) : \mathbb{R}^d \to \mathbb{R}^d, \sigma(\cdot) : \mathbb{R}^d \to \mathbb{R}^{d\times d}$ are differentiable. If no boundaries are desired, we can take $\Omega = \mathbb{R}^n$. Recall that b is entirely determined by σ, U and the requirement that the process is stationary and reversible: !!!!. We refer to Bovier[8] and Pavliotis[31] for a useful exposition on these kinds of processes.

This paper's main results arise from consideration of three related objects induced by this diffusion: the Dirichlet form, the capacity, and the Dirichlet problem.

Definition 3. *The **Dirichlet form** of X is given by*

$$\mathcal{E}(f,g) = \frac{1}{2}\int_\Omega (\sigma(x)\nabla f(x))^T(\sigma(x)\nabla g(x))e^{-U(x)}\mathrm{d}x$$

This form induces a "capacity" on pairs of nested sets:

Definition 4. *Let $A \subset \tilde{A} \subset \Omega$ be non-empty. Assume we have an open set $D \subset \Omega$ for which $\partial D = \partial A \cup \partial \tilde{A}$ and smooth. The **capacity** $\mathrm{cap}(A, \tilde{A})$ is defined as*

$$\mathrm{cap}(A,\tilde{A}) = \inf_{f\in\mathcal{H}_{A,\tilde{A}}} \mathcal{E}(f,f)$$

where $\mathcal{H}_{A,\tilde{A}}$ is the space of functions f such that

1. *$f \in H^1$, where H^1 is the Soblev space of weakly differentiable functions*
2. *$\mathcal{E}(f,f) < \infty$*
3. *$f \geqslant 1$ on ∂A and $f \leqslant 0$ on $\partial \tilde{A}$*

The capacity is intimately connected with a partial differential equation known as the Dirichlet problem:

Definition 5. *Let $A, B \subset \Omega$ be non-empty and disjoint. The **Dirichlet problem** for A, B with respect to the diffusion X is defined as the partial differential equation*

$$0 = \sum_{i=1}^{d} b_i(x) \frac{\partial f(x)}{\partial x_i} + \frac{1}{2} \sum_{i=1}^{d} \sum_{j=1}^{d} a_{ij}(x) \frac{\partial^2 f(x)}{\partial x_i \partial x_j}$$

where $a(x) = \sigma(x)\sigma(x)^T$, with boundary conditions

$$h(x) = 1, x \in A$$
$$h(x) = 0, x \in B$$

As long as there is some set $D \subset \Omega$ for which $\partial D = \partial A \cup \partial B$, this problem has a unique solution which we will denote $h_{A,B}$.

The connection between the capacity and the Dirichlet problem is given by the following, proved in Theorem 7.33 of Bovier:[8]

Proposition 1. *If $\mathcal{H}_{A,\tilde{A}} \neq \varnothing$, then*

$$\text{cap}\left(A; \tilde{A}\right) = \mathcal{E}(h_{A,\tilde{A}^c}, h_{A,\tilde{A}^c})$$

At first glance, it is unclear why any of these objects are relevant to the study of the diffusion X. The answer comes in the form of the celebrated *Dirichlet Principle*, which states that the solution to the Dirichlet problem carries the probabilistic interpretation

$$h_{A,B}(x) = \mathbb{P}(X_{\tau_{A \cup B}} \in A | X_0 = x)$$

where $\tau_S \triangleq \inf\{t \geqslant 0 : X_t \in S\}$. That is, $h_{A,B}(x)$ is the probability for X to hit A first before hitting B if we start the process at x. The Dirichlet principle is the key that connects hitting probabilities to the capacity and enables the main results of this work.

Appendix B: Proof of the Main Theorem

Assume X is a reversible stationary diffusion on Ω governed by Equation (2). Let $A \subset \tilde{A} \subset \Omega, B \subset \tilde{B} \subset \Omega$. Let $\tilde{A}, \tilde{B}$ be disjoint and $\Omega \backslash (\tilde{A} \cup \tilde{B})$ ε-flat for the hitting probabilities $h_{A,B}(x)$. Let us assume the set boundaries are all smooth.

Under these conditions, we will show we can use local capacities to get good approximations for $h_{A,B}(x)$ when $x \notin \tilde{A}, \tilde{B}$. To do so, our key idea is to uncover upper and lower bounds on the value of the Dirichlet form applied to this function, $\mathcal{E}(h_{A,B}, h_{A,B})$. We will see that these bounds can be understood in terms of capacities, and the resulting inequalities will then yield our main result in the form of Theorem 2.

Lemma 2. *The Dirichlet form of $h_{A,B}$ can be upper-bounded in terms of the capacities:*

$$\mathcal{E}(h_{A,B}, h_{A,B}) \leqslant \frac{\operatorname{cap}(A, \tilde{A}) \operatorname{cap}(B, \tilde{B})}{\operatorname{cap}(A, \tilde{A}) + \operatorname{cap}(B, \tilde{B})}$$

Proof. Per Proposition 1 and the Dirichlet principle, we have that

$$\mathcal{E}(h_{A,B}, h_{A,B}) = \operatorname{cap}(A; B^c) \leq \mathcal{E}(u, u)$$

for any $u \in \mathcal{H}_{A,B^c}$. Thus, to prove an upper bound it suffices to find functions u for which $u \in \mathcal{H}_{A,B^c}$ and we can calculate $\mathcal{E}(u, u)$. To this end, consider

$$u_c(x) \triangleq \begin{cases} (1-c)h_{A,\tilde{A}^c}(x) + c & \text{if } x \in \tilde{A} \\ c(1 - h_{B,\tilde{B}^c}(x)) & \text{if } x \in \tilde{B} \\ c & \text{otherwise} \end{cases}$$

These functions are well-suited to giving us upper bounds on $\mathcal{E}(h_{A,B}, h_{A,B})$. Indeed:

- $u_c \in \mathcal{H}_{A,B^c}$. Indeed, u_c takes a constant value c outside of $\tilde{A}, \tilde{B}$, drops smoothly to in $\tilde{B}$ to achieve 0 on ∂B, and rises smoothly in $\tilde{A}$ to achieve 1 on $\partial \tilde{A}$. Thus, since we have assumed the boundaries of $\tilde{A}, \tilde{B}$ are smooth, $u_c \in \mathcal{H}_{A,B^c}$.

- $\mathcal{E}(u_c, u_c)$ can be calculated by applying Proposition 1 twice, yielding $\mathcal{E}(u_c, u_c) = (1 - c)^2 \operatorname{cap}(A, \tilde{A}) + c^2 \operatorname{cap}(B, \tilde{B})$.

Thus the u_c functions give us a practical way to calculate upper bounds:

$$\mathcal{E}(h_{A,B}, h_{A,B}) \leq (1-c)^2 \operatorname{cap}(A, \tilde{A}) + c^2 \operatorname{cap}(B, \tilde{B})$$

This inequality holds for any value of c. To get the best bound, we can take derivatives to minimize the right hand side with respect to c. The result is

$$c^* = \frac{\operatorname{cap}\left(A; \tilde{A}\right)}{\operatorname{cap}\left(A; \tilde{A}\right) + \operatorname{cap}\left(B; \tilde{B}\right)}$$

Plugging this into the previous equation, we obtain our final result. □

Lemma 3. *Let $m = \frac{1}{2}(\sup_{x \notin \tilde{A}, \tilde{B}} h_{A,B}(x) + \inf_{x \notin \tilde{A}, \tilde{B}}(h_{A,B}(x)))$. The Dirichlet form of $h_{A,B}$ can be lower-bounded in terms of m and the capacities:*

$$\mathcal{E}(h_{A,B}, h_{A,B}) \geq \left(1 - m - \frac{\varepsilon}{2}\right)^2 \operatorname{cap}(A, \tilde{A}) \mathbb{I}_{m \leq 1 - \frac{\varepsilon}{2}} + \left(m - \frac{\varepsilon}{2}\right)^2 \operatorname{cap}(B, \tilde{B}) \mathbb{I}_{m \geq \frac{\varepsilon}{2}}$$

Proof. Recall that $\mathcal{E}(h_{A,B}, h_{A,B})$ can be expressed as an integral over Ω. We decompose this into three integrals: one over $\tilde{A}$, one over $\Omega \backslash \tilde{A}, \tilde{B}$, and one over $\tilde{B}$.

$$\mathcal{E}(h_{A,B}, h_{A,B}) = \int_{\tilde{A}} \|\sigma \nabla h_{A,B}\|^2 dx + \int_{\tilde{B}} \|\sigma \nabla h_{A,B}\|^2 dx + \int_{\Omega \backslash \tilde{A}, \tilde{B}} \|\sigma \nabla h_{A,B}\|^2 dx$$

Since the integrand is always positive, we can get a lower bound by simply ignoring the integral over $\Omega \backslash \tilde{A}, \tilde{B}$ and focusing on the integrals over $\tilde{A}, \tilde{B}$. The $\tilde{A}, \tilde{B}$ integrals can be lower-bounded using capacities.

For example, let us focus on the A case. There are two different possibilities we must consider:

- If $m > 1 - \varepsilon/2$ we will simply note that the integral over the $\tilde{A}$ region is nonnegative.
- If $m \leq 1 - \varepsilon/2$, then we define

  $$u_A(x) \triangleq \frac{h_{A,B}(x) - m - \frac{\varepsilon}{2}}{1 - m - \frac{\varepsilon}{2}}$$

  Note that $u_A \in \mathcal{H}_{A,\tilde{A}}$. Indeed, $h_{A,B}(x) = 1$ for $x \in \partial A$ and the ε-flatness condition shows that $h_{A,B}(x) \leq m + \frac{1}{2}$ for $x \in \partial \tilde{A}$. Thus, applying the definition of the capacity, we see that $\mathcal{E}(u_A, u_A) \geq \operatorname{cap}\left(A; \tilde{A}\right)$. Thus we see that

  $$\begin{aligned} \int_{\tilde{A}} \|\sigma \nabla h_{A,B}\|^2 dx &= \left(1 - m - \frac{\varepsilon}{2}\right)^2 \int_{\tilde{A}} \|\sigma \nabla u_A\|^2 dx \\ &\geq \left(1 - m - \frac{\varepsilon}{2}\right)^2 \operatorname{cap}\left(A; \tilde{A}\right) \end{aligned}$$

Putting these together, we obtain

$$\int_{\tilde{A}} \|\sigma \nabla h_{A,B}\|^2 dx \geq \left(1 - m - \frac{\varepsilon}{2}\right)^2 \operatorname{cap}\left(A; \tilde{A}\right) \mathbb{I}_{m \leq 1 - \frac{\varepsilon}{2}}$$

Applying the same ideas to the integral over $\tilde{B}$, we obtain our result. □

Theorem. *The hitting probabilities can be well-approximated by the capacities:*

$$\sup_{x \notin \tilde{A}, \tilde{B}} \left| h_{A,B}(x) - \frac{\operatorname{cap}(A, \tilde{A})}{\operatorname{cap}(A, \tilde{A}) + \operatorname{cap}(B, \tilde{B})} \right| \leqslant \varepsilon + \sqrt{\varepsilon/2}$$

Proof. To simplify notation, let $\kappa_A = \operatorname{cap}\left(A; \tilde{A}\right)$ and $\kappa_B = \operatorname{cap}\left(B; \tilde{B}\right)$. Applying the previous two lemmas, we obtain the inequality

$$\frac{\kappa_A \kappa_B}{\kappa_A + \kappa_B} \geq \left(1 - m - \frac{\varepsilon}{2}\right)^2 \kappa_A \mathbb{I}_{m \leq 1 - \frac{\varepsilon}{2}} + \left(m - \frac{\varepsilon}{2}\right)^2 \kappa_B \mathbb{I}_{m \geq \frac{\varepsilon}{2}}$$

In analyzing this inequality, there are three possibilities to consider.

- If $m \in (\epsilon/2, 1 - \epsilon/2)$, the quadratic formula yields

$$m \geqslant \frac{\kappa_A}{\kappa_A + \kappa_B} + \frac{\frac{\varepsilon}{2}(\kappa_B - \kappa_A) - \sqrt{\kappa_A \kappa_B \varepsilon (2 - \varepsilon)}}{\kappa_A + \kappa_B}$$
$$m \leqslant \frac{\kappa_A}{\kappa_A + \kappa_B} + \frac{\frac{\varepsilon}{2}(\kappa_B - \kappa_A) + \sqrt{\kappa_A \kappa_B \varepsilon (2 - \varepsilon)}}{\kappa_A + \kappa_B}$$

  Applying $\left|\frac{\kappa_B - \kappa_A}{\kappa_A + \kappa_B}\right| \leq 1$ and the fact that the geometric mean $\sqrt{\kappa_A \kappa_B}$ never exceeds the arithmetic mean $(\kappa_A + \kappa_B)/2$, it follows that

$$\left| m - \frac{\kappa_A}{\kappa_A + \kappa_B} \right| \leq \frac{\epsilon + \sqrt{\epsilon(2 - \epsilon)}}{2}$$

  Applying the fact that m was designed so that $|h_{A,B}(x) - m| < \varepsilon/2|$ for all $x \notin \tilde{A}, \tilde{B}$, we obtain

$$\left| h_{A,B} - \frac{\kappa_A}{\kappa_A + \kappa_B} \right| \leq \frac{2\epsilon + \sqrt{\epsilon(2 - \epsilon)}}{2}$$

- If $m < \varepsilon/2$, our equations become

$$\frac{\cancel{\kappa_A} \kappa_B}{\kappa_A + \kappa_B} \geq \left(1 - m - \frac{\varepsilon}{2}\right)^2 \cancel{\kappa_A}$$

  Our assumption that $m \leq \varepsilon/2$ indicates that $(1 - m - \varepsilon/2)^2 \geq (1 - \varepsilon)^2$, thus in fact we have

$$\frac{\kappa_B}{\kappa_A + \kappa_B} \geq (1 - \varepsilon)^2 = 1 + \varepsilon^2 - 2\varepsilon$$

which means that $\kappa_A/(\kappa_A+\kappa_B) \leq 2\varepsilon - \varepsilon^2 \leq 2\varepsilon$. Thus we assumed $m \in [0, \varepsilon/2]$ and showed that $\kappa_A/(\kappa_A+\kappa_B) \in [0, 2\varepsilon-\varepsilon^2]$, so it follows that

$$\left| m - \frac{\kappa_A}{\kappa_A+\kappa_B} \right| \leq 2\varepsilon - \varepsilon^2$$

and so for any $x \notin \tilde{A}, \tilde{B}$, we have

$$\left| h_{A,B}(x) - \frac{\kappa_A}{\kappa_A+\kappa_B} \right| \leq 2.5\varepsilon - \varepsilon^2$$

- If $m > 1 - \varepsilon/2$, the same bound can be achieved by arguments which are symmetric to those employed in $m < \varepsilon/2$:

$$\left| h_{A,B}(x) - \frac{\kappa_A}{\kappa_A+\kappa_B} \right| \leq 2.5\varepsilon - \varepsilon^2$$

Our final result is found by noting that all these bounds are upper-bounded by $\varepsilon + \sqrt{\varepsilon/2}$. □

Appendix C: Proof of the ε-flatness of the Toy Model

Proof of Theorem 1 We use M_t to denote a simple Brownian motion trapped inside $\Omega = \mathcal{B}(0,1)$ by reflecting boundaries. Define

$$\begin{aligned}
&\bar{u} = \mathbb{E}[u(Z)], \text{where } Z \sim \text{Uniform}(\Omega) \\
&\tilde{u}(x,t) = \mathbb{E}[u(M_t)|M_0 = x] \\
&\tilde{\tau}_M = \inf\{t : M_t \in \mathcal{B}(x_A, d_A) \cup \mathcal{B}(x_B, d_B)\} \\
&\tilde{\tau}_X = \inf\{t : X_t \in \mathcal{B}(x_A, d_A) \cup \mathcal{B}(x_B, d_B)\}
\end{aligned}$$

Note that, for our toy model X_t, since the energy landscape is flat outside $\mathcal{B}(x_A, d_A) \cup \mathcal{B}(x_B, d_B)$, $\tilde{\tau}_M | M_0 = x$ has the same distribution as $\tilde{\tau}_X | X_0 = x$, $\forall x \in \Omega/(\mathcal{B}(x_A, d_A) \cup \mathcal{B}(x_B, d_B))$. In particular, applying the Dynkin's formula, we have

$$u(x) = \mathbb{E}[u(X_{t\wedge\tilde{\tau}_X})|X_0 = x] = \mathbb{E}[u(M_{t\wedge\tilde{\tau}_M})|M_0 = x], \forall x \in \Omega/(\tilde{A} \cup \tilde{B})$$

Using the above, and the fact that $u(x) \in [0,1], \forall x \in \Omega/(\tilde{A} \cup \tilde{B})$, it's easy to see

$$\begin{aligned}
|u(x) - \tilde{u}(x,t)| &\leqslant \mathbb{E}[|u(M_{t\wedge\tilde{\tau}_M}) - u(M_t)||M_0 = x] \\
&= \mathbb{E}[|u(M_{t\wedge\tilde{\tau}_M}) - u(M_t)|\chi_{(0,t)}(\tilde{\tau}_M)|M_0 = x] \\
&\leqslant \mathbb{P}(\tilde{\tau}_M < t | M_0 = x) \\
&= \mathbb{P}(\tilde{\tau}_X < t | X_0 = x)
\end{aligned}$$

Using Lemma 4, we also have

$$\begin{aligned}|\tilde{u}(x,t)-\bar{u}| &\leqslant \left|\int_\Omega u(y)\mu_x^t(\mathrm{d}y)-\int_\Omega u(y)\pi(\mathrm{d}y)\right| \\ &\leqslant |\mu_x^t-\pi|(\Omega) \\ &= d(\mu_x^t,\pi) \\ &< \frac{2}{t}\end{aligned}$$

where $|\mu_x^t-\pi|$ is the total variation of the signed measure $\mu_x^t-\pi$.

From Lemma 5, for any fixed value of $d \geqslant 3$ and $r_{\tilde{A}}, r_{\tilde{B}}, \varepsilon > 0$, there exists a $c = c(d, r_{\tilde{A}}, r_{\tilde{B}}, \varepsilon)$ such that if $d_A, d_B < c$, then

$$\mathbb{P}\left(\tilde{\tau}_X < \frac{8}{\varepsilon} | X_0 \notin \tilde{A} \cup \tilde{B}\right) < \frac{\varepsilon}{4}$$

Likewise, for any fixed value of $d_A, r_{\tilde{A}}, d_B, r_{\tilde{B}}, \varepsilon > 0$, there exists a $c = c(d_A, r_{\tilde{A}}, d_B, r_{\tilde{B}}, \varepsilon)$, such that if the dimension $d \geqslant c$ then the same holds.

This implies that, $\forall x \notin \tilde{A} \cup \tilde{B}$

$$\begin{aligned}|u(x)-\bar{u}| &\leqslant \left|u(x)-\tilde{u}\left(x,\frac{8}{\varepsilon}\right)\right| + \left|\tilde{u}\left(x,\frac{8}{\varepsilon}\right)-\bar{u}\right| \\ &\leqslant \mathbb{P}\left(\tilde{\tau}_X < \frac{8}{\varepsilon} | X_0 = x\right) + \frac{2}{\frac{8}{\varepsilon}} \\ &< \frac{\varepsilon}{4}+\frac{\varepsilon}{4} \\ &= \frac{\varepsilon}{2} \\ \implies \sup_{x,y\notin\tilde{A}\cup\tilde{B}} |u(x)-u(y)| &< \varepsilon\end{aligned}$$

which is the desired result. □

Lemma 4. *(Uniform ergodicity) Let $\Omega = \mathcal{B}(0,1) \subset \mathbb{R}^d$, and use M_t to denote a Brownian motion trapped by reflecting boundaries inside Ω. Use π to denote the uniform distribution within Ω, which is also the equilibrium distribution of M_t. Then the distribution $\mu_x^t = \mathbb{P}(M_t \in \cdot | M_0 = x)$ converges in total variation distance to π, and we can have the uniform bound*

$$d(\mu_x^t, \pi) = \sup_{A\subset\Omega} |\mu_x^t(A) - \pi(A)| < \frac{2}{t}, \forall x \in \Omega, t > 0$$

Proof We adopt a coupling construction. Assume $M_0 = x$. Let Y_t denote another Brownian motion trapped by reflecting boundaries inside Ω, and assume $Y_0 \sim \pi$. Note that, due to

the lack of any potential, we in fact have $Y_t \sim \pi, \forall t$. Define

$$\rho_1 = \inf\{t : \|M_t\|_2 = \|Y_t\|_2\}$$
$$\alpha = \frac{M_{\rho_1} - Y_{\rho_1}}{\|M_{\rho_1}\|_2 - \|Y_{\rho_1}\|_2}$$

and further define

$$\tilde{Y}_t = \begin{cases} Y_t, t \leqslant \rho_1 \\ M_t - 2\alpha\langle\alpha, M_t\rangle, t \geqslant \rho_1 \end{cases}$$

Now take

$$\rho_2 = \inf\{t \geqslant \rho_1 : \langle\alpha, M_t\rangle = 0\}$$

and finally define

$$\widetilde{\tilde{Y}}_t = \begin{cases} Y_t, t \leqslant \rho_1 \\ M_t - 2\alpha \left\langle \alpha, M_t \right\rangle, \rho_1 \leqslant t \leqslant \rho_2 \\ M_t, \rho_2 \leqslant t \end{cases}$$

Then $\widetilde{\tilde{Y}}$ itself must carry the law of Brownian motion trapped inside of Ω with $\widetilde{\tilde{Y}}_0 \sim \pi$, and thus also satisfies $\widetilde{\tilde{Y}}_t \sim \pi, \forall t > 0$. In particular, $\forall A \subset \Omega$,

$$\begin{aligned} & |\mu_x^t(A) - \pi(A)| \\ = & |\mathbb{P}(M_t \in A) - \mathbb{P}(\widetilde{\tilde{Y}}_t \in A)| \\ = & |\mathbb{E}[\chi_A(M_t) - \chi_A(\widetilde{\tilde{Y}}_t)]| \\ \leqslant & \mathbb{P}(\rho_2 \geqslant t) \\ \leqslant & \frac{\mathbb{E}[\rho_2]}{t} \end{aligned}$$

Thus to complete the proof of the lemma, it suffices to bound $\mathbb{E}[\rho_2]$. Use W_t to denote a d-dimensional Brownian motion. Define

$$\tau^W = \inf\{t : \|W_t\| \geqslant 1\}$$

Then

$$\mathbb{E}[\tau^W | W_0 = x] = \frac{1 - \|x\|_2^2}{d} \tag{C1}$$

This can be easily verified by writing down the corresponding Possion equation for the expectation $f(x) = \mathbb{E}[\tau^W | W_0 = x]$.

$$-\frac{1}{2}\triangle f(x) = 1$$
$$f(x) = 0, \forall x \in \partial\mathcal{B}(0,1)$$

With this result, we first bound $\mathbb{E}[\rho_1]$. Define $\rho_1^M = \inf\{t : \|M_t\|_2 = 1\}$ and $\rho_1^Y = \inf\{t : \|Y_t\|_2 = 1\}$. Since $\|X_t\|, \|Y_t\| \leqslant 1, \forall t$, it follows that $\rho_1 \leqslant \rho_1^M \wedge \rho_1^Y$. Applying Equation C1, we have

$$\mathbb{E}[\rho_1] \leqslant \mathbb{E}[\rho_1^M] = \frac{1 - \|x\|_2^2}{d} \leqslant \frac{1}{d} < 1, \forall d \geqslant 3$$

To bound $\mathbb{E}[\rho_2 - \rho_1]$, we note that $\rho_2 - \rho_1$ is stochastically dominated by the time it takes a one-dimensional reflecting Brownian motion in $[-1, 1]$ to hit 0, starting at $\|x\|_2$. Using the reflection principle, we can see that this hitting time is equivalent to the first exit time from the interval $[-1, 1]$ of a one-dimensional Brownian motion starting at $1 - \|x\|_2$. Using Equation $C1$, we have

$$\mathbb{E}[\rho_2 - \rho_1] \leqslant \frac{1 - (1 - \|x\|_2)^2}{1} \leqslant 1$$

Putting these together, we have

$$d(\mu_x^t, \pi) = \sup_{A \subset \Omega} |\mu_x^t(A) - \pi(A)| < \frac{2}{t}, \forall x \in \Omega, t > 0$$

□

Lemma 5. *Define $\tilde{\tau}_X = \inf\{t : X_t \in \mathcal{B}(x_A, d_A) \cup \mathcal{B}(x_B, d_B)\}$. For any fixed value of $d \geqslant 3$ and $r_{\tilde{A}}, r_{\tilde{B}}, \varepsilon > 0$, there exists a $c = c(d, r_{\tilde{A}}, r_{\tilde{B}}, \varepsilon)$ such that if $d_A, d_B < c$, then*

$$\mathbb{P}\left(\tilde{\tau}_X < \frac{8}{\varepsilon} | X_0 \notin \tilde{A} \cup \tilde{B}\right) < \frac{\varepsilon}{4}$$

Likewise, for any fixed value of $d_A, r_{\tilde{A}}, d_B, r_{\tilde{B}}, \varepsilon > 0$, there exists a $c = c(d_A, r_{\tilde{A}}, d_B, r_{\tilde{B}}, \varepsilon)$, such that if the dimension $d \geqslant c$ then the same holds.

Proof First, observe that, for a given t,

$$\begin{aligned}\mathbb{P}(\tilde{\tau}_X < t | X_0 \notin \tilde{A} \cup \tilde{B}) = {} & \mathbb{P}(X_{\tilde{\tau}_X} \in \mathcal{B}(x_A, d_A) | X_0 \notin \tilde{A} \cup \tilde{B}) \mathbb{P}(\tilde{\tau}_X < t | X_{\tilde{\tau}_X} \in \mathcal{B}(x_A, d_A), X_0 \notin \tilde{A} \cup \tilde{B}) \\ & + \mathbb{P}(X_{\tilde{\tau}_X} \in \mathcal{B}(x_B, d_B) | X_0 \notin \tilde{A} \cup \tilde{B}) \mathbb{P}(\tilde{\tau}_X < t | X_{\tilde{\tau}_X} \in \mathcal{B}(x_B, d_B), X_0 \notin \tilde{A} \cup \tilde{B})\end{aligned}$$

If we can establish

$$\mathbb{P}\left(\tilde{\tau}_X < \frac{8}{\varepsilon} | X_{\tilde{\tau}_X} \in \mathcal{B}(x_A, d_A), X_0 \notin \tilde{A} \cup \tilde{B}\right) < \frac{\varepsilon}{4}$$

$$\mathbb{P}\left(\tilde{\tau}_X < \frac{8}{\varepsilon} | X_{\tilde{\tau}_X} \in \mathcal{B}(x_B, d_B), X_0 \notin \tilde{A} \cup \tilde{B}\right) < \frac{\varepsilon}{4}$$

Then we have proved the original result. The proofs for these two inequalities are exactly the same. In what follows, we are going to prove

$$\mathbb{P}\left(\tilde{\tau}_X < \frac{8}{\varepsilon} | X_{\tilde{\tau}_X} \in \mathcal{B}(x_A, d_A), X_0 \notin \tilde{A} \cup \tilde{B}\right) < \frac{\varepsilon}{4}$$

Intuitively, this inequality is saying that, given we start at a point outside $\tilde{A}, \tilde{B}$ and hit $\mathcal{B}(x_A, d_A)$ before hitting $\mathcal{B}(x_B, d_B)$, the probability for the hitting time to be small is small. To prove this, we pick an additional $\tilde{d}_A \in (d_A, r_{\tilde{A}})$, and consider the trajectories of X_t which start at X_0 and hit $\mathcal{B}(x_A, d_A)$ before hitting $\mathcal{B}(x_B, d_B)$. In order for $X_t$to hit $\mathcal{B}(x_A, d_A)$, it has to hit $\mathcal{B}(x_A, \tilde{d}_A)$ first. Once it hits $\mathcal{B}(x_A, \tilde{d}_A)$, there are two possibilities: either it continues to hit $\mathcal{B}(x_A, d_A)$, or it comes out of $\mathcal{B}(x_A, r_{\tilde{A}})$. When d_A becomes small or the dimension d becomes large, the probability for the process to hit $\mathcal{B}(x_A, d_A)$ before coming out of $\mathcal{B}(x_A, r_{\tilde{A}})$ is going to zero. Therefore it would take the process a lot of attempts before finally hitting $\mathcal{B}(x_A, d_A)$. Each failed attempt is associated with a certain amount of hitting time. Because of the large number of failed attempts, the accumulated hitting time would be long with high probability.

Formally, we are going to look at the behaviour of X_t in $\mathcal{B}(x_A, r_{\tilde{A}})/\mathcal{B}(x_A, d_A)$ when we start on a point $x \in \partial\mathcal{B}(x_A, \tilde{d}_A)$. Define the hitting time

$$T = \inf\{t : X_t \in \mathcal{B}(x_A, d_A) \cup \mathcal{B}(x_A, r_{\tilde{A}})^c\}$$

We care about two conditional distributions: $T||X_T - x_A| = d_A$ and $T||X_T - x_A| = r_{\tilde{A}}$. Note that because of symmetry, the starting point x won't affect these two distributions, as long as it's on $\partial\mathcal{B}(x_A, \tilde{d}_A)$. It's easy to see that, if we have a sequence of random variables

$$T_1^{\text{out}}, \cdots, T_n^{\text{out}}, \cdots \sim T||X_T - x_A| = r_{\tilde{A}}$$

a random variable

$$T^{\text{in}} \sim T||X_T - x_A| = d_A$$

and a random variable

$$N \sim \text{Geometric}(p), p = \mathbb{P}(|X_T - x_A| = d_A||X_0 - x_A| = \tilde{d}_A) = \frac{\tilde{d}_A^{2-d} - r_{\tilde{A}}^{2-d}}{d_A^{2-d} - r_{\tilde{A}}^{2-d}}$$

all independent of each other, $\forall t > 0$, we have

$$\mathbb{P}(\tilde{\tau}_X < t | X_{\tilde{\tau}_X} \in \mathcal{B}(x_A, d_A), X_0 \notin \tilde{A} \cup \tilde{B}) \leqslant \mathbb{P}\left(\sum_{n=0}^{N} T_n^{\text{out}} + T^{\text{in}} < t\right)$$

So we only need to establish bounds for $\mathbb{P}\left(\sum_{n=0}^{N} T_n^{\text{out}} + T^{\text{in}} < t\right)$. For this, we note that, $\forall s > 0$,

$$\begin{aligned}
&\mathbb{E}\left[e^{-s\left[\sum_{n=0}^{N} T_n^{\text{out}} + T^{\text{in}}\right]}\right] \\
&= \mathbb{E}\left[e^{-sT^{\text{in}}} \prod_{n=0}^{N} e^{-sT_n^{\text{out}}}\right] \\
&= \mathbb{E}[e^{-sT^{\text{in}}}]\mathbb{E}[(\mathbb{E}[e^{-sT^{\text{out}}}])^N] \\
&= \mathbb{E}[e^{-sT^{\text{in}}}] \sum_{k=0}^{+\infty} p((1-p)\mathbb{E}[e^{-sT^{\text{out}}}])^k \\
&= \frac{p\mathbb{E}[e^{-sT^{\text{in}}}]}{1-(1-p)\mathbb{E}[e^{-sT^{\text{out}}}]}
\end{aligned}$$

where $T^{\text{out}} \sim T||X_T - x_A| = r_{\tilde{A}}$.

If we can bound $\mathbb{E}\left[e^{-s\left[\sum_{n=0}^{N} T_n^{\text{out}} + T^{\text{in}}\right]}\right]$, we would then be able to bound $\mathbb{P}\left(\sum_{n=0}^{N} T_n^{\text{out}} + T^{\text{in}} < t\right)$. To bound $\mathbb{E}\left[e^{-s\left[\sum_{n=0}^{N} T_n^{\text{out}} + T^{\text{in}}\right]}\right]$, we make use of the results in Wendel[43]. Taking $n = 0$ in equation (8) and (9) in Wendel[43], we have

$$\begin{aligned}
\mathbb{E}[e^{-sT^{\text{in}}}] &= \left(\frac{d_A}{\tilde{d}_A}\right)^h \frac{I_h(\nu r_{\tilde{A}})K_h(\nu\tilde{d}_A) - I_h(\nu\tilde{d}_A)K_h(\nu r_{\tilde{A}})}{I_h(\nu r_{\tilde{A}})K_h(\nu d_A) - I_h(\nu d_A)K_h(\nu r_{\tilde{A}})} \\
\mathbb{E}[e^{-sT^{\text{out}}}] &= \left(\frac{r_{\tilde{A}}}{\tilde{d}_A}\right)^h \frac{I_h(\nu d_A)K_h(\nu\tilde{d}_A) - I_h(\nu\tilde{d}_A)K_h(\nu d_A)}{I_h(\nu d_A)K_h(\nu r_{\tilde{A}}) - I_h(\nu r_{\tilde{A}})K_h(\nu d_A)}
\end{aligned}$$

where $h = \frac{d-2}{2}$, $\nu = \sqrt{2s}$, and I_h, K_h are the modified Bessel functions of the first and second kind of order h. Using these formulas, it's easy to see that

$$\begin{aligned}
&\mathbb{E}\left[e^{-s\left[\sum_{n=0}^{N} T_n^{\text{out}} + T^{\text{in}}\right]}\right] \\
&= \frac{p\mathbb{E}[e^{-sT^{\text{in}}}]}{1-(1-p)\mathbb{E}[e^{-sT^{\text{out}}}]} \\
&= \frac{p\left(\frac{d_A}{\tilde{d}_A}\right)^h (I_h(\nu r_{\tilde{A}})K_h(\nu\tilde{d}_A) - I_h(\nu\tilde{d}_A)K_h(\nu r_{\tilde{A}}))}{(I_h(\nu r_{\tilde{A}})K_h(\nu d_A) - I_h(\nu d_A)K_h(\nu r_{\tilde{A}})) + (1-p)\left(\frac{r_{\tilde{A}}}{\tilde{d}_A}\right)^h (I_h(\nu d_A)K_h(\nu\tilde{d}_A) - I_h(\nu\tilde{d}_A)K_h(\nu d_A))}
\end{aligned}$$

To establish the desired bounds, we need some elementary properties of the modified Bessel

functions. We refer the reader to DLMF[1] for details. In particular, we have

$$\lim_{z\to 0} I_h(z) = 0 \text{ DLMF}^1 \text{ equation } 10.30.1$$
$$\lim_{z\to 0} K_h(z) = \infty \text{ DLMF}^1 \text{ equation } 10.30.2$$
$$I_h(z) = \left(\frac{1}{2}z\right)^h \sum_{k=0}^{\infty} \frac{\left(\frac{1}{4}z^2\right)^k}{k!\Gamma(h+k+1)} \text{ DLMF}^1 \text{ equation } 10.25.2$$
$$I_h(z) \sim \frac{1}{\sqrt{2\pi h}}\left(\frac{ez}{2h}\right)^h \text{as } h\to\infty \text{ DLMF}^1 \text{ equation } 10.41.1$$
$$K_h(z) \sim \sqrt{\frac{\pi}{2h}}\left(\frac{ez}{2h}\right)^{-h} \text{as } h\to\infty \text{ DLMF}^1 \text{ equation } 10.41.2$$

Using these properties, and the explicit formula for p, we can see that, when $d_A \to 0$, we have

$$p \to 0, \left(\frac{d_A}{\tilde{d}_A}\right)^h \to 0, I_h(\nu d_A) \to 0, K_h(\nu d_A) \to \infty$$

$I_h(\nu r_{\tilde{A}})K_h(\nu\tilde{d}_A) - I_h(\nu\tilde{d}_A)K_h(\nu r_{\tilde{A}})$ would remain a constant, so the numerator

$$p\left(\frac{d_A}{\tilde{d}_A}\right)^h (I_h(\nu r_{\tilde{A}})K_h(\nu\tilde{d}_A) - I_h(\nu\tilde{d}_A)K_h(\nu r_{\tilde{A}})) \to 0$$

For the denominator, we have

$$(I_h(\nu r_{\tilde{A}})K_h(\nu d_A) - I_h(\nu d_A)K_h(\nu r_{\tilde{A}})) + (1-p)\left(\frac{r_{\tilde{A}}}{\tilde{d}_A}\right)^h (I_h(\nu d_A)K_h(\nu\tilde{d}_A) - I_h(\nu\tilde{d}_A)K_h(\nu d_A))$$
$$= \left(I_h(\nu r_{\tilde{A}}) - (1-p)\left(\frac{r_{\tilde{A}}}{\tilde{d}_A}\right)^h I_h(\nu\tilde{d}_A)\right)K_h(\nu d_A) + \left((1-p)\left(\frac{r_{\tilde{A}}}{\tilde{d}_A}\right)^h K_h(\nu\tilde{d}_A) - K_h(\nu r_{\tilde{A}})\right)I_h(\nu d_A)$$

Using DLMF[1] equation 10.25.2, since we picked $\tilde{d}_A < r_{\tilde{A}}$, we have

$$\begin{aligned}
&I_h(\nu r_{\tilde{A}}) \\
&= \left(\frac{1}{2}\nu r_{\tilde{A}}\right)^h \sum_{k=0}^{\infty} \frac{\left(\frac{1}{4}\nu^2 r_{\tilde{A}}^2\right)^k}{k!\Gamma(h+k+1)} \\
&= \left(\frac{r_{\tilde{A}}}{\tilde{d}_A}\right)^h \left(\frac{1}{2}\nu\tilde{d}_A\right)^h \sum_{k=0}^{\infty} \left(\frac{r_{\tilde{A}}}{\tilde{d}_A}\right)^{2k} \frac{\left(\frac{1}{4}\nu^2\tilde{d}_A^2\right)^k}{k!\Gamma(h+k+1)} \\
&> \left(\frac{r_{\tilde{A}}}{\tilde{d}_A}\right)^h \left(\frac{1}{2}\nu\tilde{d}_A\right)^h \sum_{k=0}^{\infty} \frac{\left(\frac{1}{4}\nu^2\tilde{d}_A^2\right)^k}{k!\Gamma(h+k+1)} \\
&= \left(\frac{r_{\tilde{A}}}{\tilde{d}_A}\right)^h I_h(\nu\tilde{d}_A)
\end{aligned}$$

Since $K_h(\nu d_A) \to \infty$ and $I_h(\nu d_A) \to 0$ as $d_A \to 0$, we have the denominator goes to ∞, which implies

$$\lim_{d_A \to 0} \mathbb{E}\left[e^{-s\left[\sum_{n=0}^{N} T_n^{\text{out}} + T^{\text{in}}\right]}\right] = 0$$

When the dimension $d \to \infty$, we have $h = \frac{d-2}{2} \to \infty$ and

$$p \to 0, \left(\frac{d_A}{\tilde{d}_A}\right)^h \to 0$$

In this case, using DLMF[1] equations 10.41.1 and 10.41.2, we can see that $\mathbb{E}\left[e^{-s\left[\sum_{n=0}^{N} T_n^{\text{out}} + T^{\text{in}}\right]}\right]$ behaves like

$$\begin{aligned}
&\frac{p\left(\frac{d_A}{\tilde{d}_A}\right)^h \frac{1}{2h}\left[\left(\frac{r_{\tilde{A}}}{\tilde{d}_A}\right)^h - \left(\frac{\tilde{d}_A}{r_{\tilde{A}}}\right)^h\right]}{\frac{1}{2h}\left[\left(\frac{r_{\tilde{A}}}{d_A}\right)^h - \left(\frac{d_A}{r_{\tilde{A}}}\right)^h\right] + (1-p)\left(\frac{r_{\tilde{A}}}{\tilde{d}_A}\right)^h \frac{1}{2h}\left[\left(\frac{d_A}{\tilde{d}_A}\right)^h - \left(\frac{\tilde{d}_A}{d_A}\right)^h\right]} \\
= &\frac{p\left(\frac{d_A}{\tilde{d}_A}\right)^h}{\frac{\left(\frac{r_{\tilde{A}}}{d_A}\right)^h - \left(\frac{d_A}{r_{\tilde{A}}}\right)^h}{\left(\frac{r_{\tilde{A}}}{d_A}\right)^h - \left(\frac{\tilde{d}_A}{r_{\tilde{A}}}\right)^h} + (1-p)\left(\frac{r_{\tilde{A}}}{\tilde{d}_A}\right)^h \left[\frac{\left(\frac{d_A}{\tilde{d}_A}\right)^h - \left(\frac{\tilde{d}_A}{d_A}\right)^h}{\left(\frac{r_{\tilde{A}}}{d_A}\right)^h - \left(\frac{\tilde{d}_A}{r_{\tilde{A}}}\right)^h}\right]}
\end{aligned}$$

when h is large. Since $d_A < \tilde{d}_A < r_{\tilde{A}}$, we have

$$\lim_{h \to \infty} \frac{\left(\frac{r_{\tilde{A}}}{d_A}\right)^h - \left(\frac{d_A}{r_{\tilde{A}}}\right)^h}{\left(\frac{r_{\tilde{A}}}{\tilde{d}_A}\right)^h - \left(\frac{\tilde{d}_A}{r_{\tilde{A}}}\right)^h} = \infty$$

$$\lim_{h \to \infty} \left(\frac{r_{\tilde{A}}}{\tilde{d}_A}\right)^h \left[\frac{\left(\frac{d_A}{\tilde{d}_A}\right)^h - \left(\frac{\tilde{d}_A}{d_A}\right)^h}{\left(\frac{r_{\tilde{A}}}{\tilde{d}_A}\right)^h - \left(\frac{\tilde{d}_A}{r_{\tilde{A}}}\right)^h}\right] = 0$$

This implies that

$$\lim_{d \to \infty} \mathbb{E}\left[e^{-s\left[\sum_{n=0}^{N} T_n^{\text{out}} + T^{\text{in}}\right]}\right] = 0$$

The above arguments establish the desired bounds for $\mathbb{E}\left[e^{-s\left[\sum_{n=0}^{N} T_n^{\text{out}} + T^{\text{in}}\right]}\right]$ for both the case of $d_A \to \infty$ and the case of $d \to \infty$. These bounds in turn give us bounds for

$$\mathbb{P}\left(\sum_{n=0}^{N} T_n^{\text{out}} + T^{\text{in}} < t\right)$$

which leads to bounds for $\mathbb{P}(\tilde{\tau}_X < t | X_{\tilde{\tau}_X} \in \mathcal{B}(x_A, d_A), X_0 \notin \tilde{A} \cup \tilde{B})$. Using the same argument, we can also establish bounds for $\mathbb{P}(\tilde{\tau}_X < t | X_{\tilde{\tau}_X} \in \mathcal{B}(x_B, d_B), X_0 \notin \tilde{A} \cup \tilde{B})$. Combining these bounds, we can prove the desired result $\square$

Appendix D: Proof of the lemma

Proof of Lemma 1 The key here is to use the divergence theorem

$$\int_\Omega \nabla \cdot F(x)\mathrm{d}x = \int_{\partial\Omega} F(x)^T \mathbf{n}(x)\mathrm{d}S$$

and the property of stationary reversible SDEs (Proposition **??**)

$$J(f(x)e^{-U(x)}) = \frac{1}{2}e^{-U(x)}a(x)\nabla f(x), \forall f$$

and the fact that $\mathcal{L}(h_{A,\tilde{A}^c}(x)) = 0$.

Using these, we have

$$\begin{aligned}
\mathrm{cap}(A,\tilde{A}) &= \int_{\tilde{A}/A} \nabla h_{A,\tilde{A}^c}(x)^T a(x) \nabla h_{A,\tilde{A}^c}(x) e^{-U(x)}\mathrm{d}x \\
&= \int_{\partial\tilde{A}} h_{A,\tilde{A}^c}(x) e^{-U(x)} [a(x)\nabla h_{A,\tilde{A}^c}(x)]^T \mathbf{n}(x)\mathrm{d}S \\
&- \int_{\partial A} h_{A,\tilde{A}^c}(x) e^{-U(x)} [a(x)\nabla h_{A,\tilde{A}^c}(x)]^T \mathbf{n}(x)\mathrm{d}S \\
&- \int_{\tilde{A}/A} h_{A,\tilde{A}^c}(x) \nabla \cdot [a(x)\nabla h_{A,\tilde{A}^c}(x) e^{-U(x)}]\mathrm{d}x \\
&= -\int_{\partial A} e^{-U(x)} [a(x)\nabla h_{A,\tilde{A}^c}(x)]^T \mathbf{n}(x)\mathrm{d}S \\
&- \int_{\tilde{A}/A} h_{A,\tilde{A}^c}(x) \nabla \cdot 2J(h_{A,\tilde{A}^c}(x)e^{-U(x)})\mathrm{d}x \\
&= -\int_{\partial A} e^{-U(x)} [a(x)\nabla h_{A,\tilde{A}^c}(x)]^T \mathbf{n}(x)\mathrm{d}S \\
&- \int_{\tilde{A}/A} h_{A,\tilde{A}^c}(x) 2\mathcal{L}^*(h_{A,\tilde{A}^c}(x)e^{-U(x)})\mathrm{d}x \\
&= -\int_{\partial A} e^{-U(x)} [a(x)\nabla h_{A,\tilde{A}^c}(x)]^T \mathbf{n}(x)\mathrm{d}S \\
&- 2\int_{\tilde{A}/A} \mathcal{L}(h_{A,\tilde{A}^c}(x)) h_{A,\tilde{A}^c}(x) e^{-U(x)}\mathrm{d}x \\
&= -\int_{\partial A} e^{-U(x)} [a(x)\nabla h_{A,\tilde{A}^c}(x)]^T \mathbf{n}(x)\mathrm{d}S
\end{aligned}$$

We further have

$$
\begin{aligned}
0 &= \int_{G/A} \mathcal{L}(h_{A,\tilde{A}^c}(x)) e^{-U(x)} \mathrm{d}x \\
&= \int_{G/A} \mathcal{L}^*(h_{A,\tilde{A}^c}(x) e^{-U(x)}) \mathrm{d}x \\
&= \int_{G/A} \nabla \cdot \left(\frac{1}{2} e^{-U(x)} a(x) \nabla f(x) \right) \mathrm{d}x \\
&= \frac{1}{2} \int_{\partial G} e^{-U(x)} [a(x) \nabla h_{A,\tilde{A}^c}(x)]^T \mathbf{n}(x) \mathrm{d}S \\
&- \frac{1}{2} \int_{\partial A} e^{-U(x)} [a(x) \nabla h_{A,\tilde{A}^c}(x)]^T \mathbf{n}(x) \mathrm{d}S
\end{aligned}
$$

This implies

$$
\begin{aligned}
&\int_{\partial A} e^{-U(x)} [a(x) \nabla h_{A,\tilde{A}^c}(x)]^T \mathbf{n}(x) \mathrm{d}S \\
&= \int_{\partial G} e^{-U(x)} [a(x) \nabla h_{A,\tilde{A}^c}(x)]^T \mathbf{n}(x) \mathrm{d}S
\end{aligned}
$$

which further implies

$$
\begin{aligned}
&\mathrm{cap}(A, \tilde{A}) \\
&= - \int_{\partial G} e^{-U(x)} [a(x) \nabla h_{A,\tilde{A}^c}(x)]^T \mathbf{n}(x) \mathrm{d}S \\
&= \int_{\partial \tilde{G}} h_{G,\tilde{G}^c}(x) e^{-U(x)} [a(x) \nabla h_{A,\tilde{A}^c}(x)]^T \mathbf{n}(x) \mathrm{d}S \\
&- \int_{\partial G} h_{G,\tilde{G}^c}(x) e^{-U(x)} [a(x) \nabla h_{A,\tilde{A}^c}(x)]^T \mathbf{n}(x) \mathrm{d}S \\
&= 2 \int_{\tilde{G}/G} h_{G,\tilde{G}^c}(x) \mathcal{L}^*(h_{A,\tilde{A}^c}(x) e^{-U(x)}) \mathrm{d}x \\
&+ \int_{\tilde{G}/G} \nabla h_{G,\tilde{G}^c}(x)^T a(x) \nabla h_{A,\tilde{A}^c}(x) e^{-U(x)} \mathrm{d}x \\
&= 2 \int_{\tilde{G}/G} h_{A,\tilde{A}^c}(x) \mathcal{L}^*(h_{G,\tilde{G}^c}(x) e^{-U(x)}) \mathrm{d}x \\
&+ \int_{\tilde{G}/G} \nabla h_{G,\tilde{G}^c}(x)^T a(x) \nabla h_{A,\tilde{A}^c}(x) e^{-U(x)} \mathrm{d}x \\
&= \int_{\partial \tilde{G}} h_{A,\tilde{A}^c}(x) e^{-U(x)} [a(x) \nabla h_{G,\tilde{G}^c}(x)]^T \mathbf{n}(x) \mathrm{d}S \\
&- \int_{\partial G} h_{A,\tilde{A}^c}(x) e^{-U(x)} [a(x) \nabla h_{G,\tilde{G}^c}(x)]^T \mathbf{n}(x) \mathrm{d}S
\end{aligned}
$$

which proves the desired result. □

Appendix E: Estimating Local Hitting Probabilities

The algorithm for estimating local hitting probabilities is outlined as follows:

Algorithm 2. *Estimating $h_{A,\tilde{A}^c}(x)$ for many values of x along a shell ∂S*

Input: *$A \subset S \subset \tilde{A} \subset \Omega$ and a stationary reversible diffusion process $\{X_t\}_{t\geq 0}$ in Ω with invariant measure $\mu = e^{-U(x)}\mathrm{d}x$. We also require a series of subsets*

$$\tilde{A} \supset S_0 \supset S_1 \supset \cdots \supset S_{m-1} \supset S_m = S \supset S_{m+1} \supset \cdots \supset S_n = A$$

which indicate a kind of reaction coordinate.

Output: *A collection of points $z_1, \cdots z_{N_p}$ on ∂S sampled from the invariant measure $\mu = e^{-U(x)}\mathrm{d}x$ restricted on ∂S, along with estimates of $h_{A,\tilde{A}^c}(y_i)$ for each point.*

1. *Discretize the space.*

   (a) *Generate an ensemble of samples $z_1, \ldots, z_{N_p}$ on ∂S according to the invariant measure $\mu = e^{-U(x)}\mathrm{d}x$ restricted to ∂S.*

   (b) *Evolve the ensemble on ∂S, by repeatedly taking a random sample from $\{z_1, \ldots, z_{N_p}\}$ and follow the dynamics of $\{X_t\}_{t\geq 0}$ until the trajectory hits either ∂S_{m-1} or ∂S_{m+1}. Record the hitting locations on ∂S_{m-1} and ∂S_{m+1} until we have N_p samples on both ∂S_{m-1} and ∂S_{m+1}. Store the redundant trials for future estimation of transition probabilities.*

   (c) *Sequentially evolve the ensembles on $\partial S_{m-1}, \ldots, \partial S_2$ and on $\partial S_{m+1}, \ldots, \partial S_{n-2}$, until we have N_p samples on all of the intermediate surfaces $\partial S_1, \ldots, \partial S_{n-1}$. Store the redundant trials for future estimation of transition probabilities.*

   (d) *For each one of the surfaces $\partial S_1, \ldots, \partial S_{n-1}$, cluster the N_p samples on that surface into N_b states.*

   The result of this step is a partitioning of each shell ∂S_i into N_b discrete regions.

2. *Estimate the transition probabilities between these states by running an additional N_s local simulations for each one of the N_b states on each surface. The result of this step is an estimate of the probability of transitioning from state k on ∂S_i to state l on*

∂S_j, which we denote by $P_{k,l}^{(i,j)}$, where $k, l \in \{1, \ldots, N_b\}$ and $i, j \in \{1, \ldots, n-1\}$ with $|i - j| = 1$.

3. *Use the transition probabilities to get an estimate of the hitting probabilities for the N_b states on ∂S. In line with related works on Markov state models,[10,21,30] we approximate the continuous dynamics using closed-form calculations from the discrete Markov chain we have developed in the previous two steps. In particular, we estimate overall hitting probabilities using the standard "one-step analysis." For any $k \in \{1, \ldots, N_b\}$ and $i \in \{1, \ldots, n-1\}$, let $u_k^{(i)}$ denote the probability of hitting $\partial A = \partial S_n$ before hitting $\partial \tilde{A} = \partial S_0$ if we start the discretized process at state k on ∂S_i. We can calculate our object of interest by solving the matrix difference equation*

$$u^{(i)} = P^{(i,i+1)} u^{(i+1)} + P^{(i,i-1)} u^{(i-1)}, i = 1, \ldots, n-1$$

with boundary conditions $u^{(0)} = \mathbf{0}, u^{(n)} = \mathbf{1}$, where $\mathbf{0}$ and $\mathbf{1}$ are vectors of all 0's and 1's. This gives the estimated hitting probability for each cluster. We then estimate the hitting probability of each point z_i by

$$h_{A,\tilde{A}^c}(z_i) = u_k^{(m)}, z_i \in \text{cluster } k \text{ on } \partial S \tag{E1}$$

Appendix F: Details on Energy Function

For the energy function, we hand-designed two different kinds of landscape: random well energy, which we use for the region around target A, and random crater energy, which we use for the region around target B. The basic components of these energy functions are the well component, given by

$$F_w(x|d_w, r) = -\frac{d_w}{r^4}(||x - x_A||_2^4 - 2r^2||x - x_A||_2^2) - d_w \tag{F1}$$

where d_w gives the depth of the well; the crater component, given by

$$F_c(x|d_c, h, r) = \frac{d_c}{3b^2r^4 - r^6}(2||x - x_B||_2^2 - 3(b^2 + r^2)||x - x_B||_2^4 + 6b^2r^2||x - x_B||_2^2) - d_c \tag{F2}$$

where d_c and h give the depth and the height of the crater, respectively, and

$$b^2 = -\frac{1}{3d}(-3d_c r^2 + C + \frac{\Delta_0}{C}) \tag{F3}$$

with

$$C = 3r^2 \sqrt[3]{d_c h(d_c + \sqrt{d_c(d_c + h)})}$$
$$\Delta_0 = -9 d_c h r^4$$

and finally a random component, given by

$$F_r(x|\mu, \sigma) = \sum_{i=1}^{m} \prod_{j=1}^{d} exp(-\frac{(x_j - \mu_{ij})^2}{2\sigma_{ij}^2}) \tag{F4}$$

where $\mu = (\mu_{ij})_{m \times d}$ and $\sigma = (\sigma_{ij})_{m \times d}$, with $\mu_i = (\mu_{i1}, \cdots, \mu_{i,d}), i = 1, \cdots, m$ being the locations of m Gaussian random bumps in the region around the targets, and $\sigma_{ij}, i = 1, \cdots, m, j = 1, \cdots, d$ gives the corresponding standard deviations.

To make sure the energy function is continuous, and the different components of the energy function are balanced, we introduce a mollifier, given by

$$F_m(x|x_0, r) = exp(-\frac{r}{r - ||x - x_0||_2^{20}}) \tag{F5}$$

where $x_0 = x_A, r = d_A$ or $x_0 = x_B, r = d_B$, depending on which target we are working with, and a rescaling of the random componet, which is given by $0.1 * d_w$ if we are perturbing the well component, and $0.1 * (d_c + h)$ if we are perturbing the crater component.

Intuitively, for the well component, we use a 4th order polynomial to get a well-like energy landscape around the target that is continuous and differentiable at the boundary. Similarly, for the crater component, we use a 6th order polynomial to get a crater-like energy landscape around the target that is also continuous and differentiable at the boundary. For the random component, we are essentially placing a number of Gaussian bumps around the target. And for the mollifier, we are designing the function such that it's almost exactly 1 around the target, until it comes to the outer boundary, when it transitions smoothly and swiftly to 0. To summarize, given parameters d_w, d_c, h and random bumps μ_A, μ_B with $\mu_i^A \in \dot{A} \setminus A, i = 1, \cdots, m_A, \mu_i^B \in \dot{B} \setminus B, i = 1, \cdots, m_B$, and the corresponding standard deviations σ^A, σ^B with $\sigma_{ij}^A, i = 1, \cdots, m_A, j = 1, \cdots, d, \sigma_{ij}^B, i = 1, \cdots, m_B, j = 1, \cdots, d$, the energy function we used in the experiments is given by

$$F(x) = F_w(x|d_w, d_A) + 0.1 \times d_w \times F_m(x|x_A, d_A) + F_r(x|\mu^A, \sigma^A), \forall x \in \dot{A} \setminus A \tag{F6}$$
$$F(x) = F_c(x|d_c, h, d_B) + 0.1 \times (d_c + h) \times F_m(x|x_B, d_B) + F_r(x|\mu^B, \sigma^B), \forall x \in \dot{B} \setminus B \tag{F7}$$

In our actual experiments, we used

$$d_w = 10.0, d_c = 6.0, h = 1.0, \sigma_{ij}^A = \sigma_{k,l}^B = 0.01, \forall i, j, k, l$$

and

$$\mu^A = \begin{pmatrix} 0.512 & 0.597 & 0.009 & -0.018 & -0.009 \\ 0.496 & 0.597 & 0.009 & 0.026 & -0.013 \\ 0.464 & 0.58 & -0.018 & -0.007 & -0.012 \\ 0.528 & 0.591 & -0.029 & 0.008 & 0.022 \\ 0.469 & 0.601 & -0.022 & -0.002 & 0.014 \\ 0.517 & 0.608 & 0.013 & -0.02 & 0.021 \\ 0.474 & 0.588 & 0.005 & 0.002 & 0.003 \\ 0.532 & 0.575 & 0.018 & 0.005 & 0.01 \\ 0.466 & 0.6 & 0.012 & 0.027 & -0.004 \\ 0.497 & 0.617 & -0.006 & 0.019 & -0.033 \end{pmatrix}, \mu^B = \begin{pmatrix} -0.749 & -0.019 & -0.022 & 0.014 & 0.032 \\ -0.701 & 0.013 & 0.038 & 0.02 & 0.005 \\ -0.683 & -0.021 & -0.024 & -0.02 & 0.05 \\ -0.756 & -0.012 & 0.016 & -0.001 & 0.013 \\ -0.696 & 0.008 & 0.038 & 0.031 & -0.037 \\ -0.68 & 0.023 & -0.041 & -0.001 & -0.017 \\ -0.73 & -0.022 & 0.031 & -0.033 & 0.011 \\ -0.763 & 0.008 & 0.013 & 0.016 & 0.004 \\ -0.669 & -0.002 & -0.006 & 0.004 & -0.033 \\ -0.709 & -0.012 & 0.032 & 0.024 & -0.02 \end{pmatrix}$$

REFERENCES

[1]NIST digital library of mathematical functions. `http://dlmf.nist.gov/`.

[2]Michael Andrec, Anthony K Felts, Emilio Gallicchio, and Ronald M Levy. Protein folding pathways from replica exchange simulations and a kinetic network model. *Proc. Natl. Acad. Sci. U. S. A.*, 102(19):6801–6806, May 2005.

[3]D Aristoff, J Bello-Rivas, and R Elber. A mathematical framework for exact milestoning. *Multiscale Model. Simul.*, 14(1):301–322, January 2016.

[4]Eric B Baum. Intractable computations without local minima. *Phys. Rev. Lett.*, 57(21):2764–2767, November 1986.

[5]Juan M Bello-Rivas and Ron Elber. Exact milestoning. *J. Chem. Phys.*, 142(9):094102, March 2015.

[6]Nicholas H Bingham. Random walk on spheres. *Zeitschrift für Wahrscheinlichkeitstheorie und Verwandte Gebiete*, 22(3):169–192, 1972.

[7]Peter G Bolhuis, David Chandler, Christoph Dellago, and Phillip L Geissler. Transition path sampling: throwing ropes over rough mountain passes, in the dark. *Annu. Rev. Phys. Chem.*, 53:291–318, 2002.

[8]Anton Bovier and Frank den Hollander. *Metastability: A Potential-Theoretic Approach*. Springer, February 2016.

[9]David Chandler. Statistical mechanics of isomerization dynamics in liquids and the transition state approximation. *J. Chem. Phys.*, 68(6):2959–2970, March 1978.

[10]John D Chodera and Frank Noé. Markov state models of biomolecular conformational dynamics. *Curr. Opin. Struct. Biol.*, 25:135–144, April 2014.

[11]Markus Christen and Wilfred F van Gunsteren. On searching in, sampling of, and dynamically moving through conformational space of biomolecular systems: A review. *J. Comput. Chem.*, 29(2):157–166, January 2008.

[12]Christoph Dellago, Peter G Bolhuis, Félix S Csajka, and David Chandler. Transition path sampling and the calculation of rate constants. *J. Chem. Phys.*, 108(5):1964–1977, February 1998.

[13]Ron O Dror, Robert M Dirks, J P Grossman, Huafeng Xu, and David E Shaw. Biomolecular simulation: A computational microscope for molecular biology. *Annu. Rev. Biophys.*, 41(1):429–452, May 2012.

[14]Weinan E. and Eric Vanden-Eijnden. Towards a theory of transition paths. *J. Stat. Phys.*, 123(3):503, May 2006.

[15]Weinan E and Eric Vanden-Eijnden. Transition-path theory and path-finding algorithms for the study of rare events. *Annu. Rev. Phys. Chem.*, 61:391–420, 2010.

[16]Henry Eyring. The activated complex in chemical reactions. *J. Chem. Phys.*, 3(2):107–115, February 1935.

[17]David E Goldberg. *Genetic Algorithms in Search, Optimization and Machine Learning*. Addison-Wesley Longman Publishing Co., Inc., Boston, MA, USA, 1st edition, 1989.

[18]J M Goldberg and R L Baldwin. A specific transition state for s-peptide combining with folded s-protein and then refolding. *Proc. Natl. Acad. Sci. U. S. A.*, 96(5):2019–2024, March 1999.

[19]Adam Hospital, Josep Ramon Goñi, Modesto Orozco, and Josep L Gelpí. Molecular dynamics simulations: advances and applications. *Adv. Appl. Bioinform. Chem.*, 8:37–47, November 2015.

[20]Xuhui Huang, Yuan Yao, Gregory R Bowman, Jian Sun, Leonidas J Guibas, Gunnar Carlsson, and Vijay S Pande. Constructing multi-resolution markov state models (MSMs) to elucidate RNA hairpin folding mechanisms. *Pac. Symp. Biocomput.*, pages 228–239,

2010.

[21]Brooke E Husic and Vijay S Pande. Markov state models: From an art to a science. *J. Am. Chem. Soc.*, 140(7):2386–2396, February 2018.

[22]M Jacob, M Geeves, G Holtermann, and F X Schmid. Diffusional barrier crossing in a two-state protein folding reaction. *Nat. Struct. Biol.*, 6(10):923–926, October 1999.

[23]S Kirkpatrick, C D Gelatt, and M P Vecchi. Optimization by simulated annealing. *Science*, 220(4598):671–680, May 1983.

[24]Konstantin Klenin, Birgit Strodel, David J Wales, and Wolfgang Wenzel. Modelling proteins: conformational sampling and reconstruction of folding kinetics. *Biochim. Biophys. Acta*, 1814(8):977–1000, August 2011.

[25]J Machta. Strengths and weaknesses of parallel tempering. *Phys. Rev. E*, 80(5):056706, November 2009.

[26]J Andrew McCammon, Bruce R Gelin, and Martin Karplus. Dynamics of folded proteins. *Nature*, 267:585, June 1977.

[27]T C B McLeish. Protein folding in High-Dimensional spaces: Hypergutters and the role of nonnative interactions. *Biophys. J.*, 88(1):172–183, January 2005.

[28]Athi N Naganathan and Victor Muñoz. Scaling of folding times with protein size. *J. Am. Chem. Soc.*, 127(2):480–481, January 2005.

[29]Frank Noé, Dieter Krachtus, Jeremy C Smith, and Stefan Fischer. Transition networks for the comprehensive characterization of complex conformational change in proteins. *J. Chem. Theory Comput.*, 2(3):840–857, May 2006.

[30]Vijay S Pande, Kyle Beauchamp, and Gregory R Bowman. Everything you wanted to know about markov state models but were afraid to ask. *Methods*, 52(1):99–105, September 2010.

[31]G A Pavliotis. Stochastic processes and applications — SpringerLink. `http://link.springer.com/content/pdf/10.1007/978-1-4939-1323-7.pdf`, 2016. Accessed: 2017-11-17.

[32]Danny Perez, Blas P Uberuaga, Yunsic Shim, Jacques G Amar, and Arthur F Voter. Chapter 4 accelerated molecular dynamics methods: Introduction and recent developments. In Ralph A Wheeler, editor, *Annual Reports in Computational Chemistry*, volume 5, pages 79–98. Elsevier, January 2009.

[33]Kevin W Plaxco and David Baker. Limited internal friction in the rate-limiting step of a two-state protein folding reaction. *Proc. Natl. Acad. Sci. U. S. A.*, 95(23):13591–13596,

November 1998.

[34]Harold A Scheraga, Mey Khalili, and Adam Liwo. Protein-folding dynamics: overview of molecular simulation techniques. *Annu. Rev. Phys. Chem.*, 58:57–83, 2007.

[35]Mads R So/rensen and Arthur F Voter. Temperature-accelerated dynamics for simulation of infrequent events. *J. Chem. Phys.*, 112(21):9599–9606, May 2000.

[36]Yuji Sugita and Yuko Okamoto. Replica-exchange molecular dynamics method for protein folding. *Chem. Phys. Lett.*, 314:141–151, 1999.

[37]Wolfgang Teschner, Rainer Rudolph, and Jean Renaud Garel. Intermediates on the folding pathway of octopine dehydrogenase from pecten jacobaeus. *Biochemistry*, 26(10):2791–2796, May 1987.

[38]Titus S van Erp and Peter G Bolhuis. Elaborating transition interface sampling methods. *J. Comput. Phys.*, 205(1):157–181, May 2005.

[39]Arthur F Voter. Hyperdynamics: Accelerated molecular dynamics of infrequent events. *Phys. Rev. Lett.*, 78(20):3908–3911, May 1997.

[40]Arthur F Voter. Parallel replica method for dynamics of infrequent events. *Phys. Rev. B Condens. Matter*, 57(22):R13985–R13988, June 1998.

[41]David J Wales. Energy landscapes: calculating pathways and rates. *Int. Rev. Phys. Chem.*, 25(1-2):237–282, January 2006.

[42]A Warshel and M Levitt. Theoretical studies of enzymic reactions: dielectric, electrostatic and steric stabilization of the carbonium ion in the reaction of lysozyme. *J. Mol. Biol.*, 103(2):227–249, May 1976.

[43]J G Wendel. Hitting spheres with brownian motion. *Ann. Probab.*, 8(1):164–169, 1980.

[44]Anthony M A West, Ron Elber, and David Shalloway. Extending molecular dynamics time scales with milestoning: Example of complex kinetics in a solvated peptide. *J. Chem. Phys.*, 126(14):145104, April 2007.

[45]E P Wigner. The transition state method. In Arthur S Wightman, editor, *Part I: Physical Chemistry. Part II: Solid State Physics*, pages 163–175. Springer Berlin Heidelberg, Berlin, Heidelberg, 1997.

[46]L T Wille. Intractable computations without local minima. *Phys. Rev. Lett.*, 59(3):372, July 1987.

[47]Sichun Yang, José N Onuchic, Angel E García, and Herbert Levine. Folding time predictions from all-atom replica exchange simulations. *J. Mol. Biol.*, 372(3):756–763, September

2007.

[48]Georgeta Zemora and Christina Waldsich. RNA folding in living cells. *RNA Biol.*, 7(6):634–641, November 2010.

[49]Weihua Zheng, Michael Andrec, Emilio Gallicchio, and Ronald M Levy. Recovering kinetics from a simplified protein folding model using replica exchange simulations: A kinetic network and effective stochastic dynamics. *J. Phys. Chem. B*, 113(34):11702–11709, August 2009.